



Article

Natural Products from Red Algal Genus *Laurencia* as Potential Inhibitors of RdRp and nsp15 Enzymes of SARS-CoV-2: An In Silico Perspective

Omkar Pokharkar ¹ , Harshavardhan Anumolu ², Grigory V. Zyryanov ^{1,3,*} and Mikhail V. Tsurkan ⁴ 

¹ Department of Organic & Bio-Molecular Chemistry, Chemical Engineering Institute, Ural Federal University, Mira St. 19, 620002 Yekaterinburg, Russia; omkarpokharkar93@gmail.com

² Faculty of Science and Engineering, School of Biotechnology, Macquarie University, Sydney, NSW 2019, Australia; a.harsha2013@gmail.com

³ Postovsky Institute of Organic Synthesis of RAS (Ural Division), 22/20, S. Kovalevskoy, Akademicheskaya St., 620990 Yekaterinburg, Russia

⁴ Leibniz Institute of Polymer Research, 01005 Dresden, Germany; tsurkan@ipfdd.de

* Correspondence: gvzyryanov@gmail.com

Abstract: The genus *Laurencia*, a category of marine red algae, is well recognized for producing a large variety of natural products (NPs) that are both chemically intriguing and structurally distinct. The aim of this research was to identify NPs with potential anti-SARS-CoV-2 activity. The crystals of the proteins RdRp and nsp15 were obtained from the RCSB protein database. About 300 NPs were discovered using the PubChem, ChemSpider, and CMNPD databases. The program Autodock Vina was used to conduct the molecular docking procedure once the proteins and ligands were prepared. Before running MD simulations using the CABS-flex 2.0 website, binding affinity assessments and interactions between amino acids were carefully reviewed. Only nine NPs were shortlisted to be examined further. Bromophycolide R, S, and bromophycoic acid C show the tendency to inhibit RdRp by β -hairpin motif binding at the N-terminal known as Active site 2 (AS2), whereas the other four NPs, bromophycolide E, H, P, and thyrseol A, may effectively inhibit RdRp through interactions via C-terminal, also known as the Active site 1 (AS1). For the enzyme nsp15, bromophycoic B, C, and floridoside showed plausible interactions. In conclusion, out of nine, seven candidates shortlisted for RdRp exhibited strong interactions with the key residues in the AS1 and AS2 regions. Bromophycoic acid C may work as a dual inhibitor due to its favorable interactions with the nsp15 protein and RdRp's N-terminal, with affinities of -8.5 and -8.2 kcal/mol, respectively.

Keywords: COVID-19; SARS-CoV-2; RdRp; Nsp12; Nsp15; endoribonuclease; *Laurencia*; natural products; anti-viral; red algae



Citation: Pokharkar, O.; Anumolu, H.; Zyryanov, G.V.; Tsurkan, M.V. Natural Products from Red Algal Genus *Laurencia* as Potential Inhibitors of RdRp and nsp15 Enzymes of SARS-CoV-2: An In Silico Perspective. *Microbiol. Res.* **2023**, *14*, 1020–1048. <https://doi.org/10.3390/microbiolres14030069>

Academic Editor: Caijun Sun

Received: 30 June 2023

Revised: 26 July 2023

Accepted: 27 July 2023

Published: 31 July 2023



Copyright: © 2023 by the authors. Licensee MDPI, Basel, Switzerland. This article is an open access article distributed under the terms and conditions of the Creative Commons Attribution (CC BY) license (<https://creativecommons.org/licenses/by/4.0/>).

1. Introduction

The life-threatening coronavirus infection in 2019 was anticipated to be caused by the positive-sense, a single-strand RNA virus referred to as the severe acute respiratory syndrome coronavirus 2 (SARS-CoV-2). As of July 2023, there were over 768 million confirmed cases and about 7.0 million fatalities globally, according to the WHO dashboard <https://covid19.who.int/> (accessed on 23 July 2023). Even if the severity of the illness is lessened by existing vaccinations and antiviral medical treatment, people can still contract the illness, especially if the virus comprises unique mutations [1,2]. Moreover, vaccine efficiency is still poor, and certain antiviral medications suggested for the treatment of SARS-CoV-2 have been reported to cause viral modifications [3], making it unlikely that this will be enough to halt the spread on its own. At this point, it is quite likely that SARS-CoV-2 will spread throughout the world's population [4].

Viral RNA-dependent RNA polymerase (RdRp), also known as nonstructural protein 12 (Nsp12), is one of the many possible therapeutic targets and is regarded as a promising

target [5]. For viral replication, RdRp is essential [6]. It has conserved structural and core sequence characteristics among RNA viruses, enabling a wide range of antiviral activity [7]. In SARS-CoV-2, the RdRp complex made up of three non-structural proteins 12, 7, and 8, is necessary for RNA replication. Whilst nsp7 and nsp8 are auxiliary stimulators of polymerase activity, nsp12 functions as RdRp and is an important component [8]. There is an excellent effort being made by scientists all around the world to help elucidate feasible alternatives for inhibiting SARS-CoV-2 RdRp. Numerous studies have been conducted to date [9–47]. One medication that targets RdRp is Remdesivir, which is the only one that the US Food and Drug Administration has licensed for the treatment of COVID-19. In several clinical investigations, it has been shown that Remdesivir greatly increases COVID-19 recovery [48–50]. Remdesivir was proven to be most efficacious when provided in early infection [51,52]. Nevertheless, investigations have shown that Remdesivir did not statistically significantly outperform the standard of treatment in terms of clinical outcomes [53–55], particularly in the case of patients who had severe symptoms and required oxygen support [56]. Remdesivir may produce better results when combined with additional medications or cutting-edge therapies such as monoclonal antibodies when used alone [57,58].

A recent research investigation, again looking at the use of corticosteroids, revealed the impact on viral replication and host inflammation. It was observed that the steroid drugs Ciclesonide and mometasone showed dosage dependent influence on viral proliferation and cytotoxicity [59]. According to recent findings, Ciclesonide either directly or indirectly interacts with nsp15 [60]. A nidoviral RNA uridylylate-specific endoribonuclease is called nsp15 (NendoU). It possesses an EndoU family C-terminal catalytic domain [61]. The nsp15 was formerly believed to be involved directly in viral replication; however, it has now been discovered that this is not the case. Moreover, nsp15's ability to modulate immune system response by meddling with innate immune response has just been de-scribed [62]. It was also mentioned that nsp15 may be involved in RNA disintegration, which assists in concealing it from the host defenses. This nsp15 is described as being crucial to coronavirus biology when taking into account its different activities.

More than any other form of life, viruses have remained impervious to treatments and prevention. Only a few medications are now available to treat viral illnesses effectively. There is an increasing amount of interest in using natural products as a source for novel medications [63]. Effective medications are desperately needed to combat the SARS-CoV-2 infection, including small-molecule inhibitors [64,65], bioactive natural products [66–68], and conventional medicine [69]. Marine red algae is seen as a vital source of novel therapeutic compounds [70,71]. Natural compounds from the red algal genus *Laurencia* may prove to be vital in the treatment of SARS-CoV-2 infection due to their antiviral potency [72,73].

The purpose of this study is in silico evaluation of antiviral activity of 300 natural products from a marine red algal genus *Laurencia* (refer to Table S1). By focusing more on the amino acid interactions than just the binding affinities, this study was able to identify a small number of NPs from a total of 300 NPs [74–172]. This study is geared toward suggesting some low molecular weight NPs as potential SARS-CoV-2 RdRp (nsp12) and endoribonuclease (nsp15) inhibitors. For the RdRp enzyme, the two docking sites employed in the study are frequently referred to as active site 1 (AS1) and active site 2 (AS2); these active sites are hypothesized to be linked allosterically and coordinate the enzyme activity [173]. As there are not many studies emphasizing the relevance of docking the N-terminal (AS2), it was the major emphasis of this investigation. To ascertain if lead compounds are effective antiviral candidates, it is very crucial to take into account the activity of both AS1 and AS2 [173]. Thus, a two-phase docking strategy was used. First, the β -hairpin motif situated in the NiRAN region of the N-terminal was targeted, since it is crucial for stabilizing the complete protein and ensuring optimal functioning. Second, the top ligands shortlisted from the N-terminal docking were then further docked in the C-terminal portion of RdRp (AS1), consisting of the main catalytic core responsible for RNA replication. Finally, the toxicity and pharmacokinetic characteristics of the screened

NPs identified for both target proteins were explored. A schematic depicting the workflow used for this computational study is shown in Figure 1.

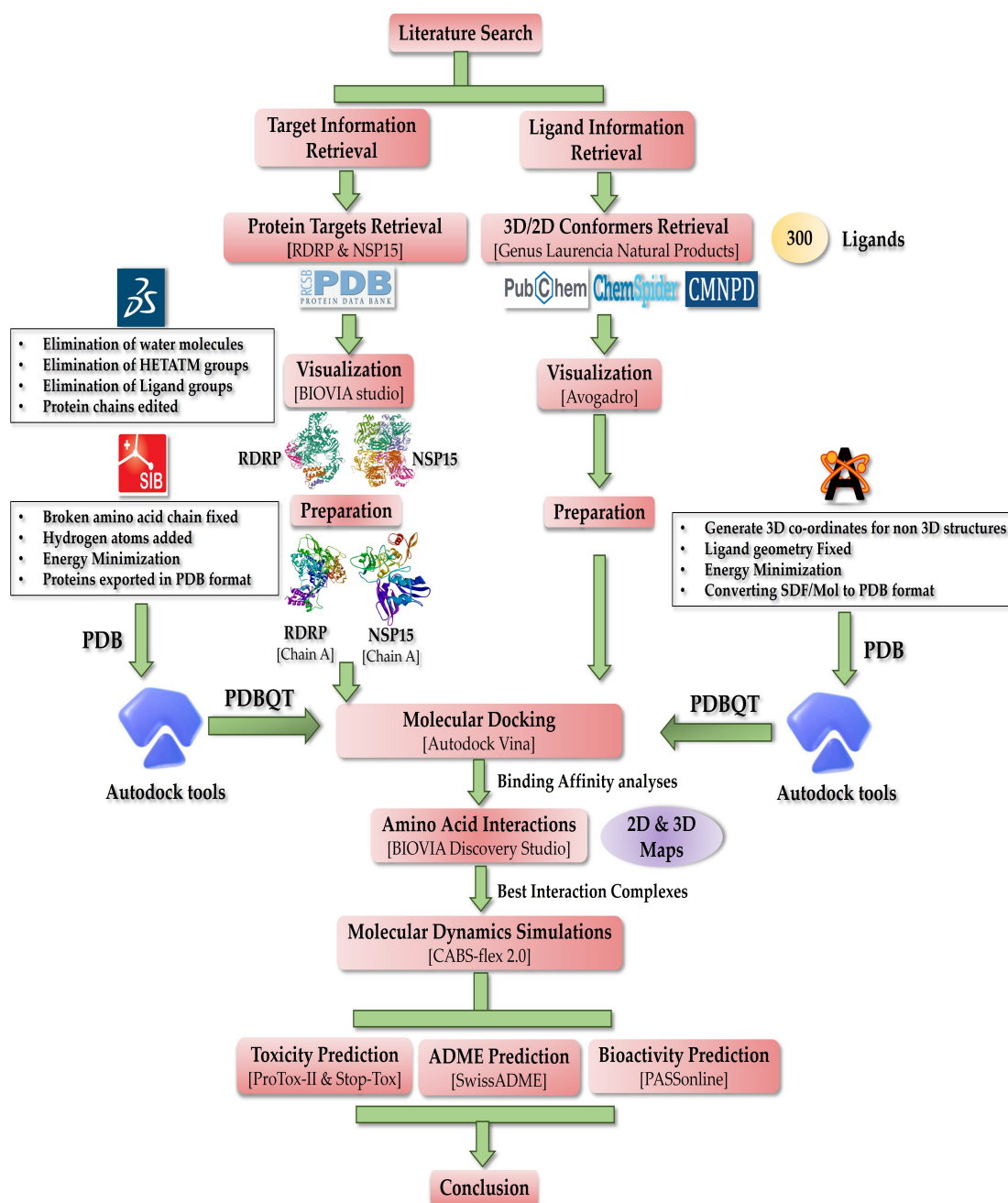


Figure 1. Schematic of the workflow describing methodology applied in this work.

2. Materials and Methods

2.1. Retrieval of Proteins

Data on the common COVID-19 proteins were found in the literature. The RCSB PDB database was used to locate the crystal structures of SARS-CoV-2 RdRp and nsp15, which were produced using electron microscopy and X-ray diffraction techniques, respectively [174]. The RNA-dependent RNA polymerase, generally known as RdRp or nsp12, and its 3D structure (PDB ID: 7BV2) resolved at 2.50 Å, were used for this investigation [175]. The 3D structure of non-structural protein number 15, also known as nsp15, which was chosen (PDB ID 6VWW), resolved at 2.20 Å [61]. The targets were selected on

the basis of resolution and PDB validation reports for optimum metrics to ensure a better docking process.

2.2. Retrieval of Ligands

A thorough literature search was conducted in order to learn more about the natural compounds produced by the *Laurencia* genus of the marine red algae. Despite the fact that there are hundreds of natural compounds, this study was restricted to about 300 naturally occurring products from this genus (refer to Table S1). To find 2D and/or 3D conformers of all 300 ligands, a thorough search was conducted. The PubChem database's 3D conformers of ligands were initially obtained in SDF chemical format [176]. In the event that 3D structures were not available, 2D conformers were downloaded. The ligands that were absent from the PubChem database were obtained from the ChemSpider database and retrieved in the Mol chemical format using the same database [177]. The 2D Mol format structures of ligands that were not accessible in the PubChem or ChemSpider databases were obtained using the CMNPD database [178].

2.3. Visualization Tools

Using BIOVIA Discovery Studio Visualizer 4.5, the protein structures of RdRp and nsp15 were studied [179]. This gave us the necessary details on the quantity of amino acid chains, connected ligands, HETATM groups, etc. However, Avogadro software was first employed for visualization and afterwards for the preparation of ligands [180,181].

2.4. Pre-Docking Preparations

Using the data gathered throughout the visualization process, BIOVIA Discovery Studio Visualizer prepared both target proteins. The nsp15 protein only had chains A and B, but the RdRp protein contained three amino acid chains, such as A, B, and C. Both proteins demonstrated the presence of ligand groups, HETATM, and water molecules. However, RdRp was also found to have a nucleic acid group. In order to get rid of unnecessary molecules (H₂O, HETATM, nucleic acid, and undesired amino acid chains), 3D structures were cleaned and trimmed. For both proteins to be utilized in this investigation, Chain A was chosen, but the ligand group was left intact. Hydrogen atoms were also added, energy minimization was performed, and Swiss-pdb viewer software [182] was utilized to perhaps restore the fragmented amino acid chain. After the energy minimization procedure, the ligand groups were eliminated; this step was important to prevent potential disruption of the active site. Additionally, these structures were stored in the Swiss-pdb viewer's PDB format before being converted utilizing Autodock tools to the necessary PDBQT format [183].

The Avogadro program was used to construct the 2D and 3D conformers of ligands acquired in SDF and Mol chemical formats. The 2-dimensional structures were first opened in Avogadro to generate 3D coordinates, which turned them into 3-dimensional structures. All 2D structures were thus transformed to 3D conformers and stored. Once all 300 products had been converted to 3D, each one was individually put through a process of geometry optimization and energy minimization. All ligands that were processed were exported in PDB format. Finally, Gasteiger charges were added using the auto dock tools by converting ligands from PDB to PDBQT format.

2.5. Docking Protocol Validation

By re-docking the original ligand RTP (remdesivir triphosphate) in the catalytic domain on the C-terminal, the docking technique was validated. On the crystal structure of the protein that was re-docked with the native RTP, the original crystal structure (PDB ID: 7BV2) was superimposed. Analyses were performed on the map of amino acid interactions and docking score was noted. To evaluate the precision of the employed protocol, the RMSD value was determined (see Figure 2).

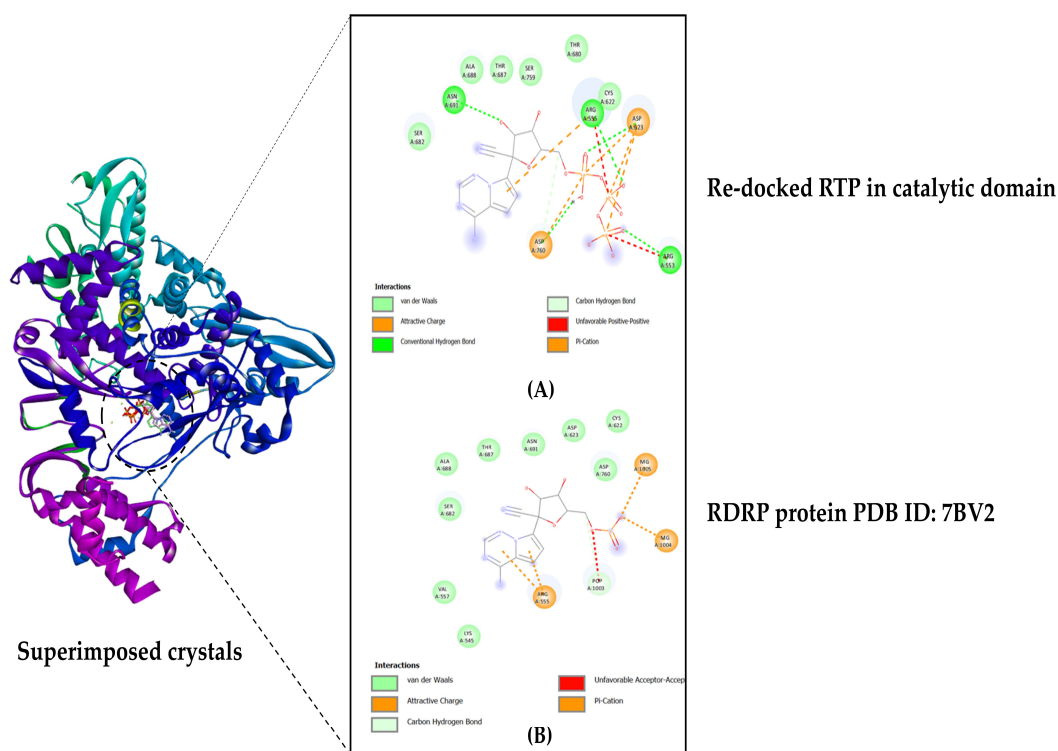


Figure 2. Docking validation: (A) RTP re-docked in the active site pocket located in the C-terminal; (B) Original protein crystal from RCSB PDB, ID: 7BV2.

2.6. Molecular Docking

For the rigid protein flexible ligand molecular docking approach, Autodock Vina 1.2.0 was employed [184,185]. The Grid box was constructed and positioned suitably using knowledge of key amino acids and active sites for RdRp and nsp15. The RdRp protein file in PDBQT format was first opened in the program, and 300 ligands were individually docked (see Table 1). RdRp's cavity volume was 1248 Å³, whereas the nsp15 protein's active site volume was 83 Å³. For RdRp phase 1 docking, the grid box was constructed over the β-hairpin motif and positioned at X = 113 Å, Y = −87 Å, Z = 79 Å. In the phase 2 docking, the top NPs identified in phase 1 docking were docked in the grid box placed at the catalytic core region X = 99 Å, Y = 96 Å, Z = 104 Å. In the case of nsp15 protein, grid box was placed at X = −93 Å, Y = 19 Å, Z = −27 Å. The nsp15 protein was also docked with all 300 ligands (see Table 2). To confirm the correctness of the outcome, the full docking process was carried out twice. Additionally, all protein–ligand complexes in PDB format were acquired in order to use BIOVIA Discovery Studio Visualizer 4.5 to show amino acid interactions (see Table 3) in 2D and 3D maps (see Figures 3–6).

2.7. MD Simulation

Using the CABS-flex 2.0 website, MD simulations were performed for protein–ligand complexes exhibiting the desired amino acid interactions [186]. This service effectively assesses protein flexibility using quick simulations. PDB files for the best complexes were posted to the server. The server gave default settings for the simulation parameters, which included the number of cycles (50), cycles between trajectory frames (50), simulation temperature (1.4), and seed for the random number generator. At default settings, these MD simulation sessions are considered equivalent to 10 ns of computer performed simulations. Root Mean Square Fluctuation (RMSF) plots were produced by simulation sessions which were used further in this study (see Figures 7–9 and Tables S13–S15).

2.8. Toxicity Profile Assessment

ProTox II and StopTox web servers were employed to assess the potential toxicity of the top-ranking ligands [187,188]. ProTox-II reduces the requirement for animal testing by making quick predictions about a tiny molecule's potential toxicity in a virtual environment. Important details regarding the ligands, including *LD50* values (mg/kg body weight), toxicity class, and toxicity endpoints (hepatotoxicity, carcinogenicity, immunotoxicity, mutagenicity, and final cytotoxicity), were given by this website (see Table 4). Estimates of the likelihood that ligands may cause acute toxicity are quickly and accurately provided by the user-friendly program StopTox. Acute oral, dermal, and inhalation toxicity information, as well as information on the likelihood of skin and eye irritation and corrosion, skin sensitization, and other critical information, were all provided by this server (refer to Table 5).

2.9. Pharmacokinetics Analysis

The canonical SMILES (Table S16, ESI) on the Swiss-ADME service was used to investigate the drug-like qualities of natural compounds that had previously been selected as the best [189]. The five Lipinski parameters (Ro5) were observed and recorded as the first act of observation. These criteria included the molecular weight (≤ 500), consensus log *p*-value (≤ 5), and the number of hydrogen bond donors and acceptors (≤ 5). Two more criteria were included—as the topological polar surface area (≤ 140) and the number of rotatable bonds (≤ 10)—in order to more accurately assess the likelihood that the ligand will be orally active (refer to Table 6). Further, the water solubility, bioavailability, and GI absorption probability were noted (see Table 7). A simple mathematical equation that produced the absorption percentage was used to more precisely measure GI absorption [190,191]:

$$AB\% = 109 - (0.345 \times TPSA)$$

Additionally, the Swiss-ADME boiled egg graph was used to analyze the cell permeability of NPs (see Figure 10). Finally, utilizing the PASS online webserver [192], possible biological activity prediction was carried out (in Table 8).

3. Results and Discussion

3.1. Binding Affinity Studies

Due to the significant number of NPs used in this investigation, the data for the binding affinity for both RdRp and nsp15 were separated into three groups. First, the classes of ligands with low affinity were those having docking scores between -4.0 and -4.9 kcal/mol and -5.0 and -5.9 kcal/mol. Second, it was considered that the ligands having docking values between -6.0 and -7.9 kcal/mol were of intermediate affinity. These low and moderate ligands were further placed in subcategories, whereas high-affinity ligands were the final group.

3.1.1. Docking β -Hairpin Motif Region (RdRp): N-Terminal

The NiRAN region and the palm subdomain of RdRp are linked by a β -hairpin motif. This motif stabilizes the overall protein structure of RdRp, aiding in its optimum functioning. Important amino acids in this region are TYR: 32, LYS: 47, TYR: 122, TYR: 129, HIS: 133, ASN: 138, ASP: 140, THR: 141, SER: 709, and ASN: 781 [193–196]. Targeting this region might inhibit RdRp by disruption of conformational dynamics triggered by ligand binding. In simple terms, there might be structural re-arrangements that ultimately alter the protein function [197]. The residue TYR: 129 from AS2 (N-terminal) and SER: 709 from AS1 (C-terminal) are conserved among all coronaviruses. Targeting these residues will most likely compromise the inter-domain connections, which will eventually have a detrimental effect on the activity of RNA synthesis [173]. The results of the phase 1 docking process for the β -hairpin motif of RdRp were divided into the three major groups.

Ten NPs made up the first grouping in the low category because they had the lowest docking scores for the RdRp protein (see Table 1). The affinities of laurencenyne, halomon, and 9-octadecanoic acid were the lowest at -4.0 kcal/mol. 6, 8-cycloeudesmane had the greatest affinity score, which was closely followed by 1-methyl-2, 3 and 5-tribromoindole at -4.9 and -4.8 kcal/mol, respectively (refer to Table S2, ESI). The second subgroup had about 172 NPs, 19 of which had a low docking value of -5.0 kcal/mol. Nevertheless, only five of the NPs in this group showed the maximum docking scores in this class, which was -5.9 kcal/mol (refer to Table S3, ESI). These were (6*R*, 9*R*, 10*S*)-10-bromo-9-hydroxychamigra-2, 7(14)-diene, aldingenin C, axinyson B, aplysiolic acid, and compositacin C, J. There were two subcategories within the moderate class. As well, 61 NPs with lower-moderate scores were put in the first sub-category, 20 of which had affinities of -6.0 kcal/mol; nevertheless, five NPs, including 11,14-dihydroaplysia-5,11,14,15-tetrol, *beta*-sitosterol, callophycoic acid I, cholest-5-en-3-*alpha*-ol, and saringosterol, had the lowest score in the group at -6.9 kcal/mol (refer to Table S4, ESI). The second subcategory of upper-moderate ligands included 39 NPs, of which 6 NPs had a low docking score of -7.0 kcal/mol while 4 NPs, namely *beta*-cryptoxanthin, brassicasterol, bromophycoic acid E, and bromophycolide A, displayed -7.9 kcal/mol affinity (refer to Table S5, ESI). Ultimately, we identified 18 NPs in category 3 with the greatest affinities (see Table 1). Lithothamin A had the greatest docking score for RdRp of any ligand, with a value of -9.0 kcal/mol, followed closely by dehydrothysiferol, bromophycolide S, callicladol, and bromophycolide E, which had values of -8.9 , -8.8 , -8.7 , and -8.5 kcal/mol, respectively (Table S6, ESI).

Table 1. Docking output for the N-Terminal β -hairpin region of RdRp enzyme.

RdRp Protein				
Low		Moderate		High
-4.0 to -4.9 kcal/mol	-5 to -5.9 kcal/mol	-6 to -6.9 kcal/mol	-7 to -7.9 kcal/mol	-8.0 kcal/mol and Above
1-methyl-2,3,5-tribromoindole	(-)-3-(<i>E</i>)-bromomethylidene-10 <i>beta</i> -bromo- <i>beta</i> -chamigrene	1,2-Dehydro-3,4-epoxyalisadin B	5- <i>alpha</i> -cholestane-3,6-dione	Bromophycoic acid B
6,8-cycloeudesmane	(+)-3-(<i>Z</i>)-bromomethylidene-10 <i>beta</i> -bromo- <i>beta</i> -chamigrene	2-Hydroxyluzofuranone A, B	6-hydroxycholest-4-en-3-one	Bromophycoic acid C
9-octadecanoic acid	(5 <i>S</i>)-5-Acetoxy- <i>beta</i> -bisabolene	3 <i>alpha</i> -hydroperoxy-3-epiapsin	10-acetoxyangasol	Bromophycolide E
14-methylpentadecanoic acid	(6 <i>R</i> ,9 <i>R</i> ,10 <i>S</i>)-10-bromo-9-hydroxychamigra-2,7(14)-diene	3-Bromo-4,5-dihydroxybenzaldehyde	10- <i>epi</i> -Dehydrothysiferol	Bromophycolide H
<i>beta</i> -Synderol	(10 <i>R</i>)-10-Bromo- <i>alpha</i> -chamigrene	3-Bromobarekoxide	13-Hydroxyperthysenol A	Bromophycolide K
Halomon	2-bromospironipol	3- <i>epi</i> -Perforenone A	15,16-Dehydrovenustatriol	Bromophycolide L
Luzonensin	(3 <i>Z</i>)-laurenyne	3 <i>R</i> ,4 <i>S</i> -luzonolone	15-Dehydroxythysenol A	Bromophycolide P
Hordenine	3,4-epoxyalisadin B	3 <i>S</i> ,4 <i>R</i> -luzonolone	16-Hydroxydehydrothysiferol	Bromophycolide R
Laurencenyne	3,7-dihydroxydihydrolaurene	5-acetoxypalisadin B	<i>Beta</i> cryptoxanthin	Bromophycolide S
Trans-Laurencenyne	3- <i>alpha</i> -Hydroxydehydroaplysin	5- <i>alpha</i> -Hydroxyaplystatin	Brassicasterol	Callicladol
	3- <i>beta</i> -Hydroperoxyaplysin	9-hydroxy-3- <i>epi</i> -perforenone A	Bromophycoic acid A, D, E	Dehydrothysiferol
	4-Hydroxy-1,8- <i>epi</i> -isotenerone	11,14-dihydroaplysia-5,11,14,15-Tetrol	Bromophycolide A-D, E, J, M-O, Q, T, U	Isodehydrothysiferol
	4-hydroxypalisadin C	15-hydroxypalisadin A	Callophycoic acid C-E	Laurebiphenyl
	5-acetoxyoachamigrene	Acetylmapalene A, B	Campesterol	Lithothamin A
	5- <i>epi</i> -maneolactone	Aldingenin D	Cholest-4-en-3,6-dione	Mammeisin
	7-acetyl-aplysiol	Aplysistatin	Dehydrovenustatriol	Thysenol A
	7-hydroxylarene	Aristolan-10-ol-9-one	Lactodehydrothysiferol	Thysenol B
	8,10-dibromoaplysin	Aplysidiol	Neurymenolide A, B	Thysiferol
	9-Deoxyelatal	Barekoxide	Neorietetrol	
	10-Bromo- <i>beta</i> -chamigrene	<i>beta</i> -Sitosterol	Predehydrovenustriolacetate	
	10-Bromosaplyin	Bromophycolide G, I	Prethysenol A	
	10-hydroxyisolaurene	Caespitol	Pseudodehydrothysiferol	
	10-Hydroxyaplysin	Callophycoic acid A, B, G, H, I, J	Stigmasterol	
	12-hydroxy Isolaurene	Callophycol A, B		
	12-Hydroxypalisadin B	Chamigrene Lactone		
	15-Hydroxylarene	Compositacin B, E, F, I, N		
	15-Oxolaurene	Cholest-4-en-3-one		
	Almadioxide	Cholest-5-en-3- <i>alpha</i> -ol		
	Aromadendrene	Cholest-5-en-3- <i>beta</i> -ol		
	Aldingenin A, B, C	Debromoisocalenzanol		
	Allolaurinterol	Japonenyne A		
	Allolaurinterolacetate	Johnstonol		
	Aplysinol	Laurecomin A, D		
	Aristolan-8-en-1-one	Laurenokomarin		
	Aristolane	Laurepoxylene		
	Axinyson B	Laureacetol C		
	Aplysiol-7-one	Laurefurenyne B		
	Aplysiolic acid	Laurinterolacetate		
	(-)-Bisezakylene A	Luzondiol		
	Brasilenol	Majapolene A		
	Bromocuparene	Oryzalexin S		
	Bromocyclococanol	Pacifenol		
	Bosseopentanoic acid	Palisadin D		
	Bromolaurenidifin	Perforenone A		
	Caespitane	Saringosterol		
	Caesspitenone	Tiomanene		
	Cycloeudesmol			
	Cyclolaurenol			
	Callophycoic acid F			
	Callenzanol			
	Chamigrene epoxide			
	Chinzallene			
	Compositacin A, C, D, G, H, J, K, L, M			

Table 1. Cont.

RdRp Protein					
Low		Moderate		High	
−4.0 to −4.9 kcal/mol	−5 to −5.9 kcal/mol	−6 to −6.9 kcal/mol	−7 to −7.9 kcal/mol	−8.0 kcal/mol and Above	
	Cycloelatanene A, B Cycloisallolaurinterol Chlorofucin Cupalaurenol Dactylene Debromoaplysin Debromoepiapsin Debromolaurinterol Debromolaurinterolacetate Dendroidiol Dendroidone Deoxyrepacifenol Deschloroelatal Elatenyne Elatal Epiapsin Epibrasilenol Floridoside Filiformin Filiforminol Guimarediol Heterocladol Intricenyn Isocapsitol Isodihydrolauren Isolaurellene Isolaureatin Isolaurene Itomanindole A Isolaurenidifin Isoafricanol Isoallolaurinterol Isoapsin Isodactylone A Isodebromolaurinterol Isolaurenol Isoobtusol Isopalisol Isorigidol Kumausallene Laurallene Laureacetal A, B Laurefurenyne A, C, D, E, F Laurencial Laurendecumallene A, B Laurendecumenyne A, B Laurenenyne Laurensol Laurenone A Laureoxanyne Laurecomin B, C Laurencomposidiene Laurene Laurentistich-4-ol Laureperoxide Laurokamurene A-D Luzofuran Luzonenone Luzonensol Luzonensol acetate Laurepinnacin Laurinterol Ma'iliohydrin Mailione Majapolene B Microcladallene A-C Neoisoprelaurefucin Neolaurellene Nidificene Notoryne Octadecanedioic acid Obtusane Okamurene A-E Omaezallene Oxachamigrene Palisadin A-C Pannosane Pannosanol Perforatone Perforenol Repacifenol Prelaureatin Rhodophytin Scopariol Seco-Laurokamurone Spirolaurenol Trans-Deacetylumausyne Trans-Kumausyne				

3.1.2. Validation of RdRp Catalytic Domain Docking Protocol

After being re-docked, the original inhibitor remdesivir triphosphate gave a binding affinity score of -7.1 kcal/mol, and the RMSD value for the superimposed crystal structures was calculated to be 1.51 Å. The computed RMSD value was below the threshold of 2.0 Å, indicating that the docking operation was conducted with good precision (see Figure 2).

3.1.3. Docking Catalytic Domain (RdRp): C-Terminal

After addressing active site 2 (N-terminal), we proceeded to move on to the active site 1 (C-terminal) to determine the applicability of already filtered compounds in step 1. This dual-step docking assisted in narrowing down the pool of candidates in a systematic but progressive fashion. In addition, the likelihood of discovering potent inhibitors that might bind and favorably interact with both AS1 and AS2 increased. The AS1 consists of two catalytic motifs. The first motif includes amino acid residues from 611–626. Out of which, the ASP: 618 is of paramount importance, as it is the most conserved residue. On the other hand, the second motif consists of residues ranging from 753–767. The three catalytic residues such as SER: 759, ASP: 760, and ASP: 761 are considered crucial for RdRp activity [198,199]. The highest docking score of -8.2 kcal/mol was seen for bromophycoic acid B and callicladol, whereas bromophycolide L obtained the lowest value, -7.0 kcal/mol. All results for the C-terminal docking are presented in Table S7, ESI of the supplemental information.

3.1.4. Docking nsp15

The docking process produced the output listed (in Table 2) for the endoribonuclease enzyme (nsp15) of SARS-CoV-2.

Seven NPs were found to have the lowest docking scores to the endoribonuclease protein. Halomon exhibited the lowest result, which was -4.2 kcal/mol. Bosseopentanoic and octadecanedioic acids had the strongest binding score in this category, at -4.9 kcal/mol (refer to Table S8, ESI). The second low-class subcategory had 110 NPs, 15 of which displayed the maximum docking values in this group. Nevertheless, at -5.0 kcal/mol, floridoside and laurefurenyne A had the lowest ability for binding (refer to Table S9, ESI). There were around 111 NPs in the first subcategory of the moderate class, and 41 of them displayed the lowest docking scores in the group. Nevertheless, the highest binding scores were demonstrated by five NPs, including allolaurinterol, aplysiadiol, callophycoic acid G, isolaurerisol, and mammeisin, with a -6.9 kcal/mol value (refer to Table S10, ESI). Additionally, 42 NPs made up the upper-moderate category. The absolute minimum affinity score for this group, -7.0 kcal/mol, was displayed by 11 NPs. The maximum binding value was displayed by two NPs, 15, 16-dehydrovenustatriol, and bromophycoic acid E, with a value of -7.9 kcal/mol (refer to Table S11, ESI). Lastly, the final category included the remaining 30 NPs (see Table 2). With -8.7 and -8.6 kcal/mol, respectively, bromophycolide T and 5 α -cholestane-3, 6-dione showed the maximum binding potential in this group. Ten NPs, however, showed docking scores of -8.0 kcal/mol only (refer to Table S12, ESI).

Table 2. Docking output for nsp15 enzyme.

Categorization of Ligands—nsp15				
Low		Moderate		High
−4.0 to −4.9 kcal/mol	−5 to −5.9 kcal/mol	−6 to −6.9 kcal/mol	−7 to −7.9 kcal/mol	−8.0 kcal/mol and Above
9-Octadecanoic acid 14-Methylpentadecanoic acid Bosseopentanoic acid Halomon Hordenine Octadecanedioic acid Tiomanene	1-Methyl-2,3,5-tribromindole 2-Bromopirionipol 3,4-epoxypalisadin B 3- α -Hydroxydebroaplysin 4-Hydroxy-1,8- ϵ -isotenerone 5-Acetoxyoxachamigrene 5-Acetoxypalisadin B 6,8-Cycloeuodesmane 7-Acetyl-aplysiol 9-Deoxyelatalol 10-Bromo-beta-chamigrene Aristolan-8-en-1-one Aristolan-10-ol-9-one Aristolane Almadioxide Aromadendrene Aplysiol-7-one Aplysiolic acid beta-Synderol Brasilenol (−)-BisezakyleneA Callenzanol	(−)-3-(E)-Bromomethylidene-10-beta-bromo-beta-chamigrene (+)-3-(Z)-Bromomethylidene-10-beta-bromo-beta-chamigrene (5S)-5-Acetoxy-beta-bisabolene (6R,9R,10S)-10-Bromo-9-hydroxychamigra-2,7(14)-diene (10R)-10-Bromo- α -chamigrene 1,2-Dehydro-3,4-epoxypalisadin B 2-Hydroxyluzofuranone B 3,7-dihydroxydihrolaurene 3-beta-Hydroperoxyaplysin 3-Bromo-4,5-dihydroxybenzaldehyde 3- ϵ -PerforenoneA 3R,4S-Luzonolone 3S,4R-Luzonolone (3Z)-Laurenyne 3-Bromobarekoxide 4-Hydroxypalisadin C 5- ϵ -Maneolactone 7-Hydroxylaurene 8,10-Dibromoisoaplysin 9-Hydroxy-3- ϵ -perforenone A 10-Acetoxyangasol 10-Bromosoaplysin	2-Hydroxyluzofuranone A 3- α -Hydroperoxy-3-epiaplysin 5- α -Hydroxyaplysiatin 10- ϵ -Dehydrothysiferol 11,14-Dihydroaplysia-5,11,14,15-tetrol 13-Hydroxyprathyrenol A 15,16-Dehydrovenustatriol Aplysiatin Beta cryptoxanthin Bromophycoic acid A, D, E Bromophycolide A–F, H, I, J, M, N, R Barekoxide Bromophycolide S Callophycoic acid A, C, D–F, H, I Cholest-5-en-3- α -ol Dehydrovenustatriol Isodehydrothysiferol Lactodehydrothysiferol Neurymenolide B Predehydrovenustatriolacetate Prathyrenol A Pseudodehydrothysiferol	5- α -Cholestane-3,6-dione 6-hydroxycholest-4-en-3-one 15-Dehydrothysiferol A 16-Hydroxydehydrothysiferol Brassicasterol beta-sitosterol Bromophycoic acid B Bromophycolide G Bromophycoic acid C Bromophycolide K Bromophycolide L Bromophycolide O Bromophycolide P Bromophycolide Q Bromophycolide T Bromophycolide U Callicladol Callophycoic acid B Campesterol Cholest-4-en-3,6-dione Cholest-4-en-3-one Cholest-5-en-3-beta-ol

Table 2. Cont.

Categorization of Ligands—nsp15				
Low		Moderate		High
−4.0 to −4.9 kcal/mol	−5 to −5.9 kcal/mol	−6 to −6.9 kcal/mol	−7 to −7.9 kcal/mol	−8.0 kcal/mol and Above
	Chamigrene epoxide Chinzallene Compositacin A, D-H, L, M, N Cycloelatanene A, B Cycloeludesmol Cyclolaurenol Dactylene Debromoepiapiylinol Dendroidiol Dendroidone Deoxyrepacifenol Deschloroelatal Elatol Epibrasilenol Elatenyne Floridoside Guimarediol Heterocladol Isolaurenidifidin Isoafricanol Isoaplysin Isodactyloxene A Isoobtusol Isopalisol Isorigidol Intricienye Isolaurallene Itomanindole A Kumausallene Laurecomin B, C Laurenokomarin Luzondiol Luzonensin Luzonensol Luzonensolacetate Laurallene Laureacetal B, C Laurefurenyne A, B, D, E, F Laurenecyene Laurencial Laurendecumallene A, B Laurendecumenyne B Laurenecyene Laurenisol Laureoxanyne Laurepinnacin Ma'ilohydrin Mailione Microcladallene A-C Neoisoprelaurefucin Neolaurallene Nidificene Obtusane Okamurene C, E Omaezallene Pacifenol Palisadin B, C, D Pannosane Perforatone Perforenol Prelaureatin Rhodophytin Scopariol <i>trans</i> -Deacetylumausyne <i>trans</i> -Kumausyne <i>trans</i> -Laurenecyene	10-Hydroxyaplysin 10-hydroxyisolaurene 12-hydroxy Isolaurene 12-Hydroxypalisadin B 15-hydroxypalisadin A 15-Hydroxylaurene 15-Oxolaurene Acetylmapapolene A Acetylmapapolene B Aldingenin A-D Allolaurinterol Allolaurinterolacetate Aplysinol Axinyson B Aplysidiol Bromocyclococanol Bromolaurenidifidin Bromocuparene Callophycoic acid G, J Callophycol A, B Chamigrene Lactone Compositacin B, C, I, J, K Cycloisallolaurinterol Chlorofucin Cupalaurenol Caespitane Caespitol Caesspitone Debromoisocalenzanol Debromolaurinterol Debromolaurinterolacetate Debromoaplysin Epiaplysinol Filiformin Filiforminol Isoallolaurinterol Isodebromolaurinterol Isolaurenisol Isocaesitol Isodihydrolaurene Isolaureatin Isolaurene Japonenyne A Johnstonol Laurecomin A, D Laurencomposidiene Laurene Laurentistich-4-ol Laureperoxide Laurepoxylene Laurinterolacetate Laurokamurene A-D Luzofuran Luzonenone Laurinterol Laureacetal A Laurefurenyne C Laurendecumenyne A Laurenone A Majapolene A, B Mammeisin Neoirietraol Notoryne Okamurene A, B, D Oxachamigrene Oryzalexin S Palisadin A Pannosanol Perforenone A Prepacifenol Seco-Laurokamurone Spirolaurenone	Saringosterol	Dehydrothyriferol Laurebiphenyl Lithothamin A Neurymenolide A Stigmaterol Thyrserol A Thyrserol B Thyrseriferol

3.2. Selection of Best Interaction Complexes—RdRp and nsp15

High binding affinities must not be the only factor used to determine a ligand's ability to inhibit druggable targets. Understanding the interactions between the residues is crucial to determine the potential success of the ligands in inhibiting the activity of RdRp and nsp15.

3.2.1. Selection Criteria

1. It must interact with the majority of catalytic amino acids;
2. It must form many hydrogen bonds with catalytic amino acids ($\text{RMSD} \leq 3.00$);
3. For electrostatic connections, the pre-specified threshold RMSD cutoff distance ($\text{\AA} \leq 5.00$) must not be exceeded.

3.2.2. Rejection Criteria

1. No interactions with key amino acids;
2. No hydrogen bonds are connected to important residues or exceeded $\text{RMSD} \geq 3.00$;
3. Mostly Van der Waals forces are involved in the interactions;
4. For electrostatic bonding, the maximum pre-defined RMSD cutoff distance ($\text{\AA} \leq 5.00$) was surpassed.

3.3. Best Interaction Complexes—RdRp and nsp15

Following the aforementioned selection terms and conditions, only 10 docked complexes met our criteria for ideal residue interactions for RdRp and nsp15 out of a total of 618 protein–ligand complexes. Figure 3 showcases the selected ideal docked complexes.

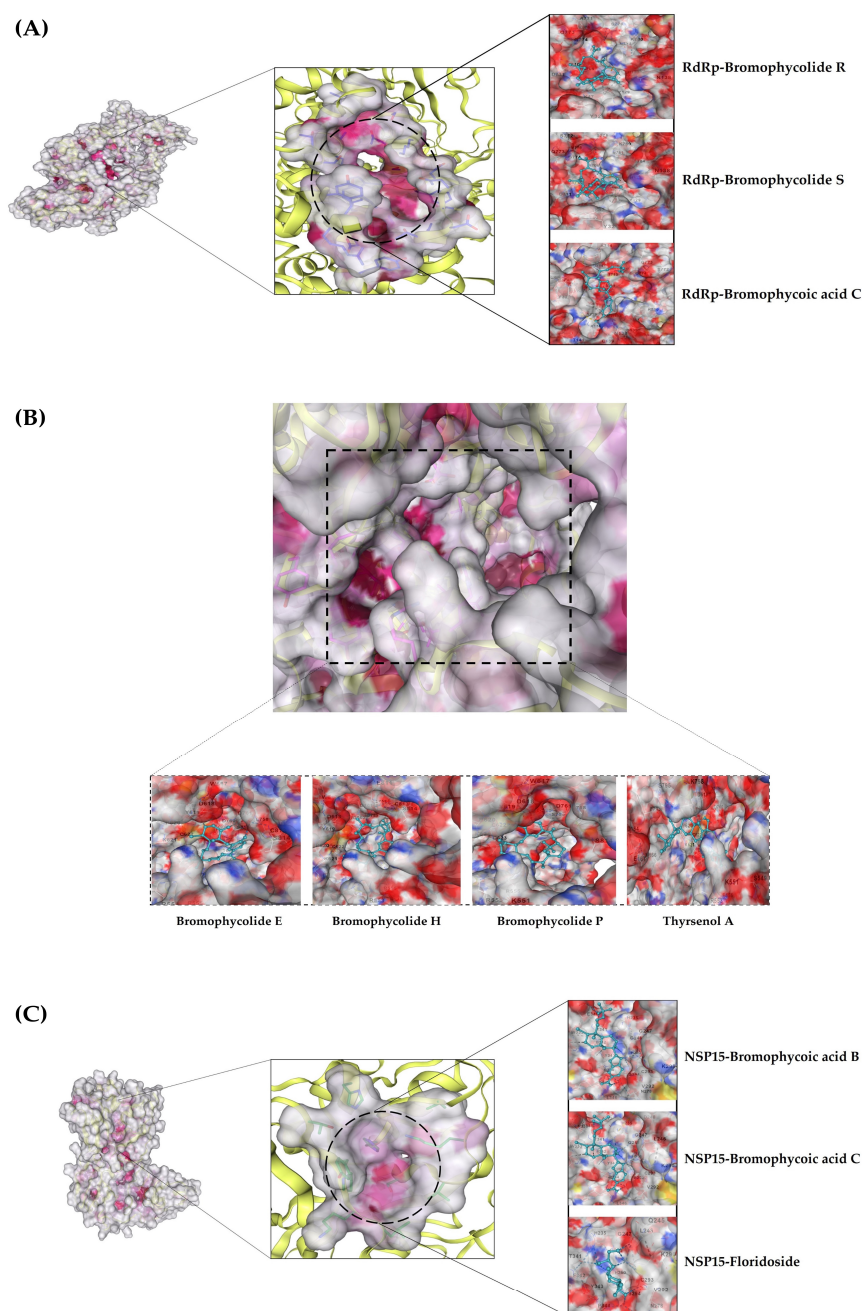


Figure 3. All shortlisted NPs: (A) RdRp β -hairpin motif in complex with three NPs; (B) RdRp C-Terminal catalytic core in complex with four NPs; (C) Enzyme nsp15 in complex with three NPs.

In the case of RdRp (β -hairpin motif), three NPs showed desirable interaction with most crucial amino acids. First, the bromophycolide R interacted strongly with seven key residues out of ten (see Figure 4 and Table 3). It interacted with SER: 709 (2.40 Å) and ASN: 781 (2.47 Å) by forming hydrogen bonds. Pi-Pi T-shaped bonds were formed with TYR: 129 (4.26 Å) and HIS: 133 (4.76 Å). Alkyl and pi-alkyl bonds were seen for TYR: 32 (4.20 Å) and LYS: 47 (3.95 Å). Van der Waals interaction was observed for ASN: 138 residue. Second, the bromophycolide S also interacted with seven residues of interest out of ten. Hydrogen bonds were formed with SER: 709 (2.00 Å) and ASN: 781 (2.66 Å). Pi-Pi T-shaped bond was formed only with TYR: 129 (4.33 Å). Furthermore, alkyl and pi-alkyl bonds were formed with two residues, TYR: 32 (4.20 Å) and LYS: 47 (3.95 Å). Lastly, HIS: 133 and ASN: 138 interacted via VdW forces. Ultimately, the third, bromophycic acid C, showed interactions with six desired residues out of ten. Two residues, TYR: 129 formed a hydrogen bond (2.39 Å) and a Pi-Pi T-shaped connection (4.14 Å). However, SER: 709 (2.56 Å) formed hydrogen bonds. Pi-cation and pi-alkyl bonds were observed to be forming connections with LYS: 47 (Å = 4.33, 4.25 respectively). Lastly, with TYR: 32 residue, it formed two alkyl bonds (4.72, and 4.79 Å).

N-terminal RdRp-Ligand complexes

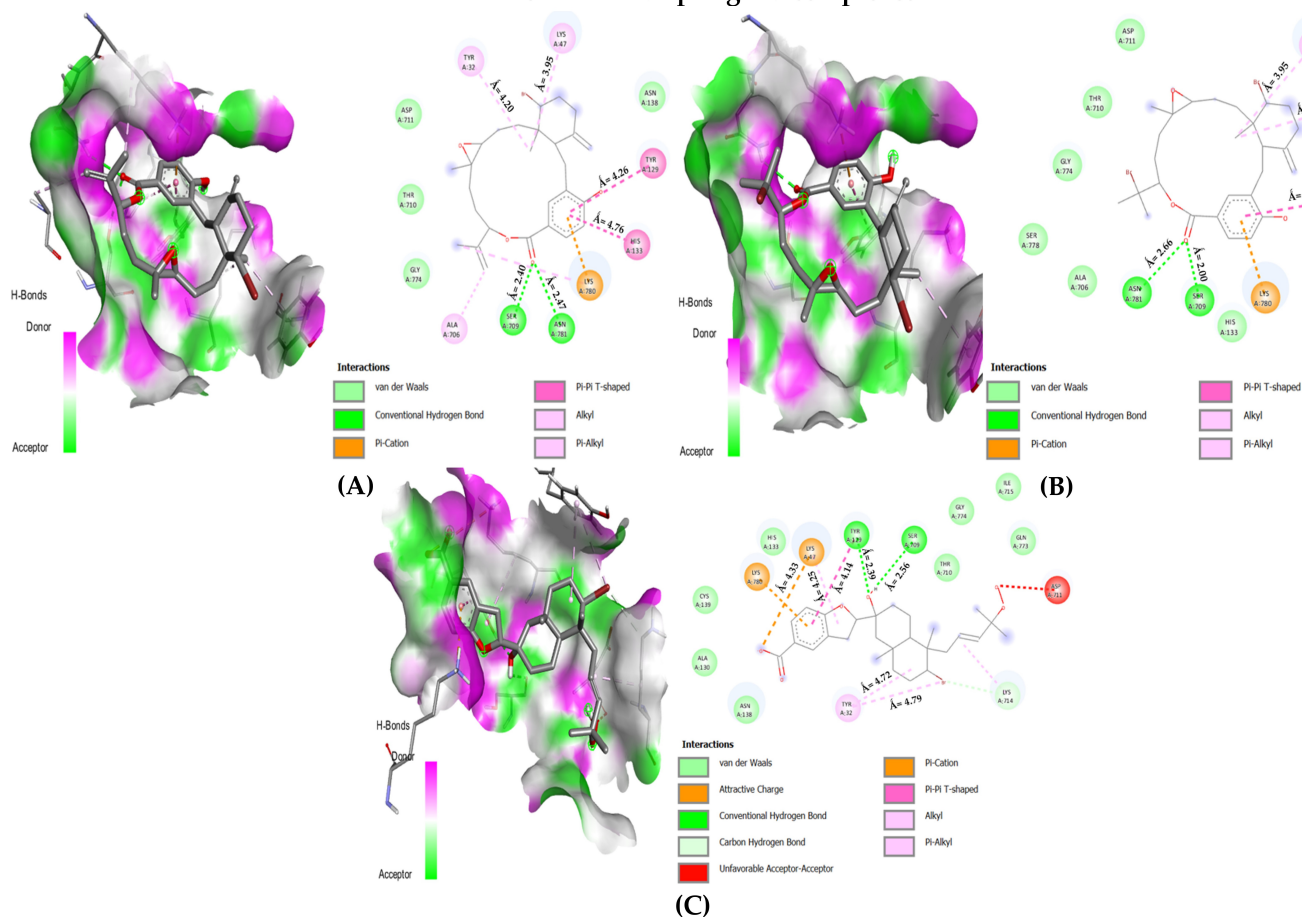


Figure 4. The 2D interaction maps for phase 1 docking: (A) RdRp β -hairpin domain–bromophycolide R complex; (B) RdRp β -hairpin domain–bromophycolide S complex; (C) RdRp β -hairpin domain–bromophycic acid C complex.

Table 3. Amino acid interaction profile of filtered nine NPs.

Favourable Residue Interactions	
Filtered Ligands	Involved Amino Acids
RdRp (N-Terminal β-Hairpin Motif)	
Bromophycolide R	TYR32 LYS47 TYR129 HIS133 ASN138 ALA706 SER709 THR710 ASP711 GLY774 LYS780 ASN781
Bromophycolide S	TYR32 LYS47 TYR129 HIS133 ASN138 ALA706 SER709 THR710 ASP711 GLY774 SER778 LYS780 ASN781
Bromophycic acid C	TYR32 LYS47 TYR129 ALA130 HIS133 ASN138 CYS139 SER709 THR710 ASP711 LYS714 ILE715 GLN773 GLY774 LYS780
RdRp (C-terminal catalytic core)	
Bromophycolide E	ARG553 ARG555 ASP618 TYR619 PRO620 CYS622 ASP623 THR680 SER682 THR687 ALA688 ASN691 LEU758 SER759 ASP760 ASP761 CYS813
Bromophycolide H	ARG553 ARG555 ASP618 LYS621 CYS622 ASP623 LEU758 SER759 ASP760 ASP761 CYS813
Bromophycolide P	ARG553 ARG555 ASP618 TYR619 PRO620 LYS621 CYS622 ASP623 ASP760 ASP761 SER814
Thyrsenol A	ARG555 ASP618 TYR619 PRO620 LYS621 CYS622 ASP623 THR687 ALA688 ASN691 LEU758 SER759 ASP760 ASP761 CYS813
nsp15 enzyme	
Bromophycic acid B	HIS235 GLY247 GLY248 HIS250 LYS290 VAL292 CYS293 SER294 TRP333 GLU340 THR341 TYR343 PRO344 LYS345 LEU346
Bromophycic acid C	HIS235 GLY247 GLY248 HIS250 LYS290 VAL292 CYS293 SER294 TRP333 GLU340 THR341 TYR343 PRO344 LYS345 LEU346
Floridoside	HIS235 GLN245 LEU246 GLY247 GLY248 HIS250 LYS290 VAL292 CYS293 SER294 THR341 PHE342 TYR343

In Figure 5, the bromophycolide E in complex with the catalytic domain of RdRp interacted with ASP: 761 and 760 by forming a single hydrogen bond (2.42 Å) and an electrostatic connection (3.50 Å). In addition, ASP: 618 and SER: 759 interacted via Van der Waals forces. Furthermore, bromophycolide H formed a hydrogen bond with ASP: 761 (2.89 Å). Hydrophobic interactions were evident for the residues ASP: 618, 760, and SER: 759. Bromophycolide P interacted with ASP: 761 and 618 using hydrophobic interactions, whereas ASP: 760 interacted electrostatically, forming a pi-anion bond (3.26 Å). However, no interactions with amino acid SER: 759 occurred. Ultimately, thyrsenol A formed a couple of hydrogen bonds (2.12 Å, 2.69 Å) with ASP: 618 and SER: 759, respectively. A carbon–hydrogen link (3.55 Å) was observed with the residue ASP: 618, whereas ASP: 761 interacted via Van der Waals forces only.

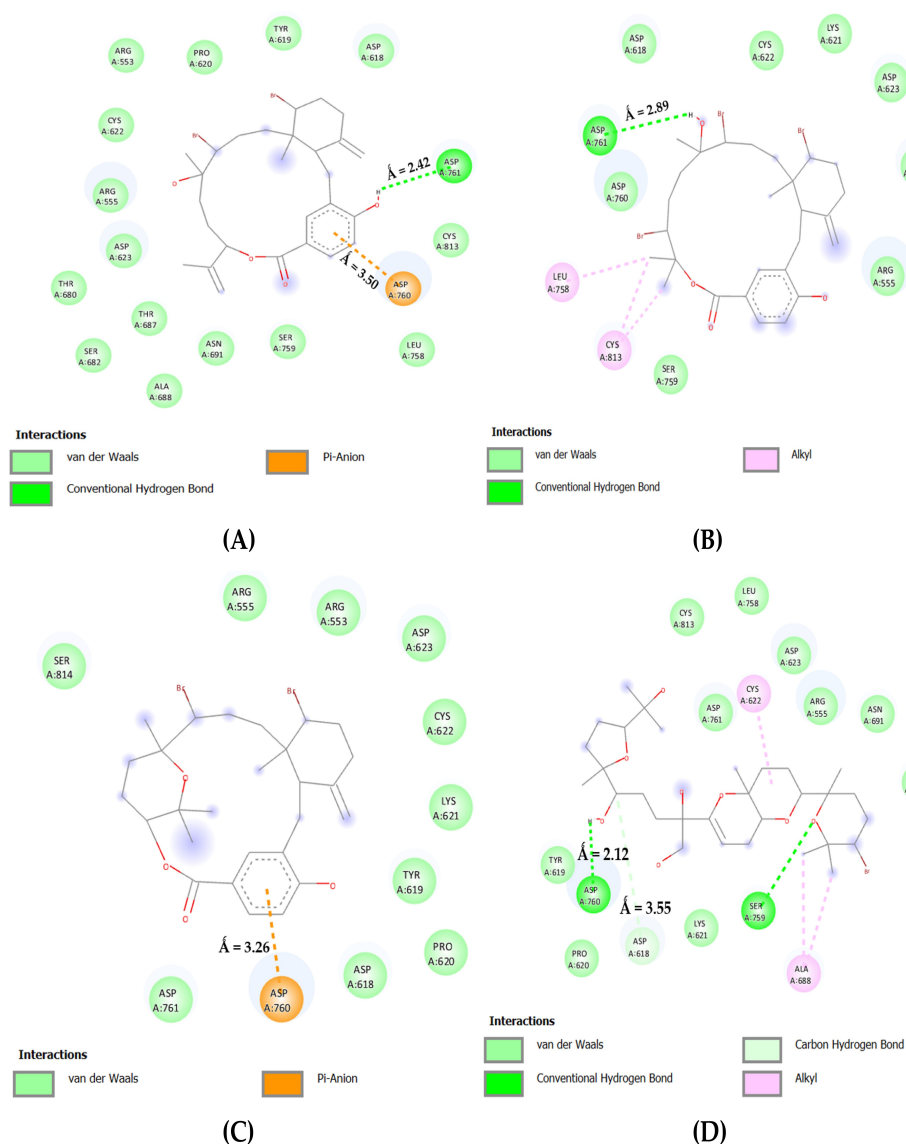


Figure 5. The 2D interaction maps for phase 2 docking: (A) RdRp C-Terminal-bromophycolide E complex; (B) RdRp C-Terminal-bromophycolide H complex; (C) RdRp C-Terminal-bromophycolide P complex; (D) RdRp C-Terminal-Thyrsenol A complex.

In Figure 6, for the nsp15 enzyme, three NPs showed the most favorable interactions by associating with four key amino acids out of eight (see Figure 3 and Table 5). First, the bromophycoic acid B formed hydrogen bonds with LYS: 290 (1.95 Å) and SER: 294 (2.35 Å). With HIS: 235, it formed one hydrogen (2.95 Å) and three pi-alkyl bonds (4.07, 4.47, and 5.00 Å). Moreover, HIS: 250 was connected with C-H bond (3.40 Å) and a pi-alkyl bond (4.46 Å). Second, the bromophycoic acid C formed hydrogen bonds with LYS: 290 (1.84 Å) and SER: 294 (2.42 Å). HIS: 235 was found to be linked by three pi-alkyl bonds (4.09, 4.33, and 4.40 Å), whereas HIS: 250 was connected by a C-H bond (3.42 Å) and a pi-alkyl bond (4.49 Å). Lastly, floridoside formed four hydrogen bonds with three residues, namely, LYS: 290 (2.26 and 2.58 Å), SER: 294 (1.94 Å), and HIS: 235 (2.31 Å). Van der Waals interactions were observed in the case of HIS: 250 residue.

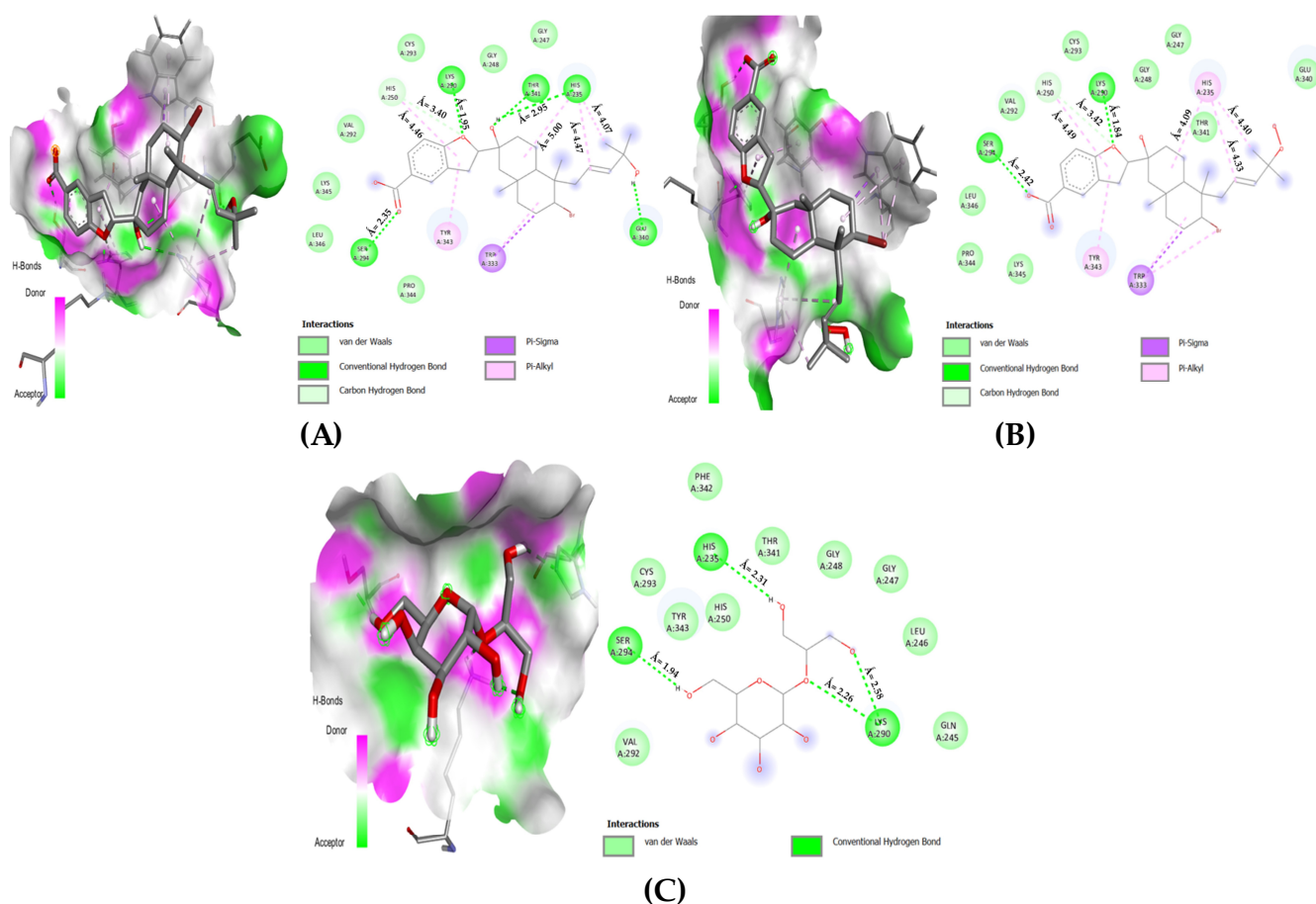


Figure 6. The 2D interaction maps for nsp15 protein: (A) nsp15 endoribonuclease–bromophycoic acid B complex; (B) nsp15 endoribonuclease–bromophycoic acid C complex; (C) nsp15 endoribonuclease–floridoside complex.

3.4. MD Simulations

The CABS-flex 2.0 tool displays good fit with NMR spectroscopic data on protein flexibility and is very efficient for fast simulations of protein residue flexibility.

MD Simulations for Selected RdRp and nsp15 Complexes

The aforementioned complexes were subjected to molecular dynamics simulations on the free to access CABS-flex 2.0 webserver. Multiple *in silico* studies concerning SARS-CoV-2 used this webserver for MD simulations, indicating its reliability [200–203].

In the case of bromophycolide R in complex with the N-terminal domain, RMSF score of 0.388 Å was obtained for the residue number ASN: 781, whereas the highest fluctuation was seen for ASN: 138 (1.606 Å). Similarly, for the complex of RdRp–bromophycolide S, the highest fluctuation (1.027 Å) was seen again for the amino acid ASN: 138. On the other hand, the lowest fluctuation was for HIS: 133 (0.159 Å). Likewise, the complex with bromophycoic acid C, TYR: 129 residue showed minimum fluctuation (0.169 Å). However, ASN: 138 fluctuated the highest (1.562 Å) of all residues (see Figure 7 and Table S13).

The C-terminal docking with bromophycolide E revealed that amino acid ASP: 761 had the lowest RMSF score of 0.139 Å, whereas the highest RMSF score of 0.7600 was seen for the ASP: 618 residue. In the case of bromophycolide H, it was observed that SER: 759 fluctuated the most (0.901 Å) and ASP: 761 residue fluctuated the least (0.540 Å). Finally, for both bromophycolide P and thyrserenol A, the least fluctuating amino acid was ASP: 761 (0.345 Å, 0.257 Å, respectively). On the other hand, the highest RMSF score of 0.594 Å and 0.498 Å for fluctuation was evident for SER: 759 residue (refer to Figure 8 and Table S14).

For the endoribonuclease enzyme (nsp15), the complexes formed with floridoside and bromophycoic acid B and C showed the highest fluctuating residue number HIS: 242. For bromophycoic acid C, the amino acid HIS: 242 fluctuated the most (2.726 Å), almost reaching the maximum limit of 3.0 Å. The lowest fluctuation was observed for the residue SER: 294 for the complexes of bromophycoic acid B (0.172 Å) and floridoside (0.134 Å). However, HIS: 249 was the lowest fluctuating residue (0.388 Å) for the nsp15–bromophycoic acid C. All complexes were concluded to be stable, as the threshold of 3.0 Å was not surpassed (see Figure 9 and Table S15). All RMSF values were well below the threshold of 3.0 Å. Thus, all 10 complexes were considered to form stable conformations.

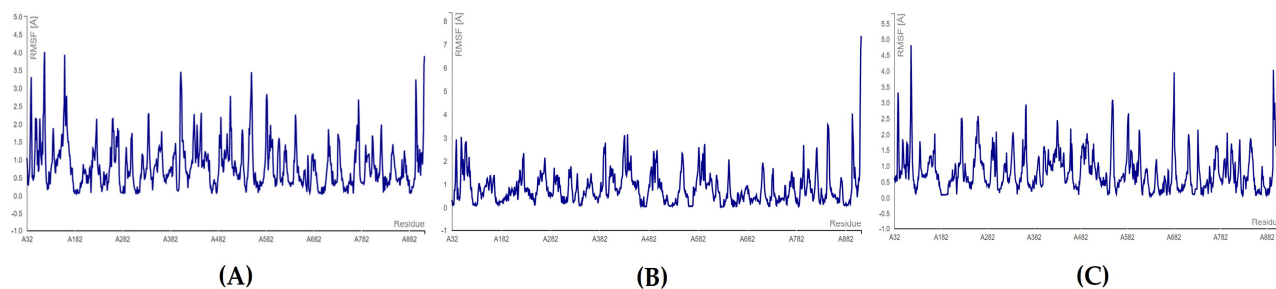


Figure 7. RMSF plots for N-terminal docking of RdRp: (A) RdRp β-hairpin–bromophycolide R complex; (B) RdRp β-hairpin–bromophycolide S complex; (C) RdRp β-hairpin–bromophycoic acid C complex.

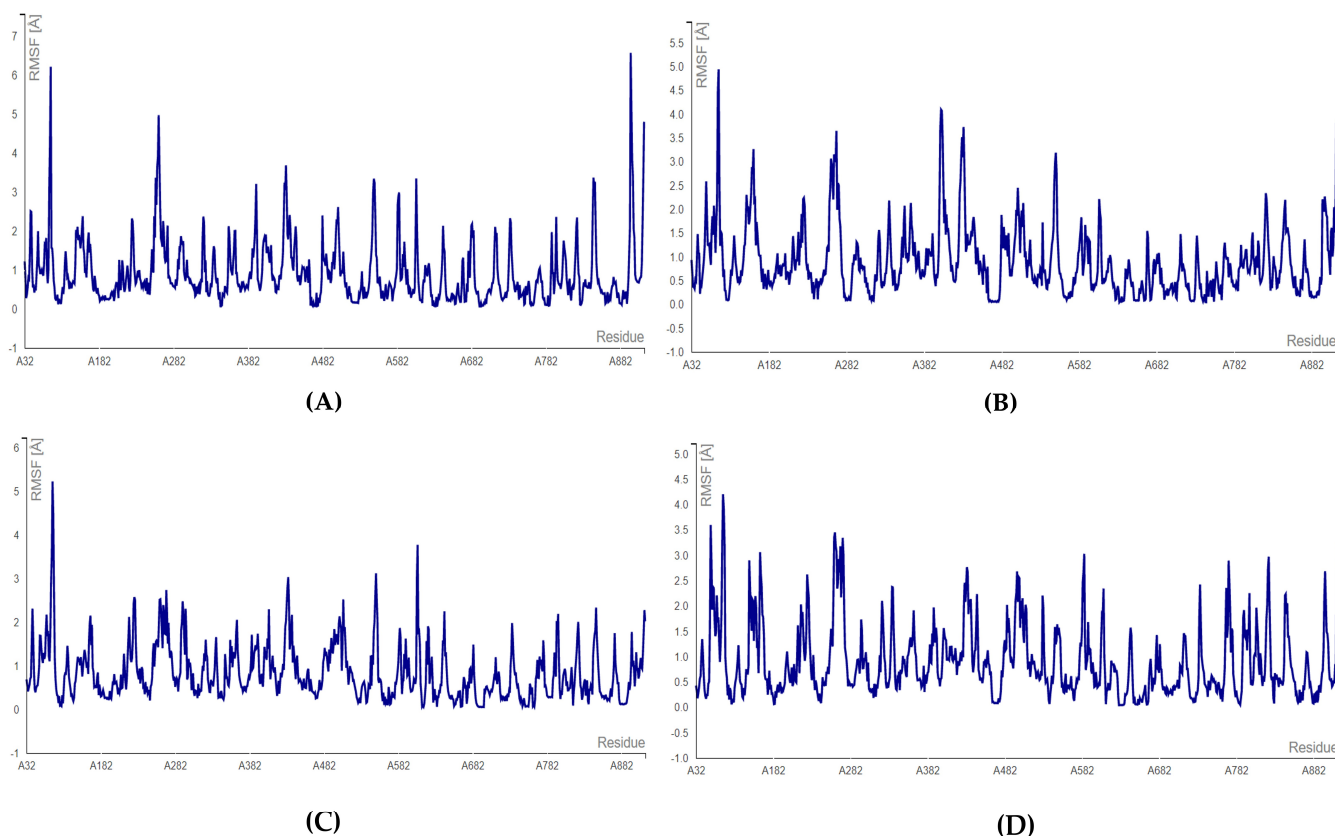


Figure 8. RMSF plots for C-terminal docking of RdRp: (A) RdRp–bromophycolide E complex; (B) RdRp–bromophycolide H complex; (C) RdRp–bromophycolide P complex; (D) RdRp–thyrseol A complex.

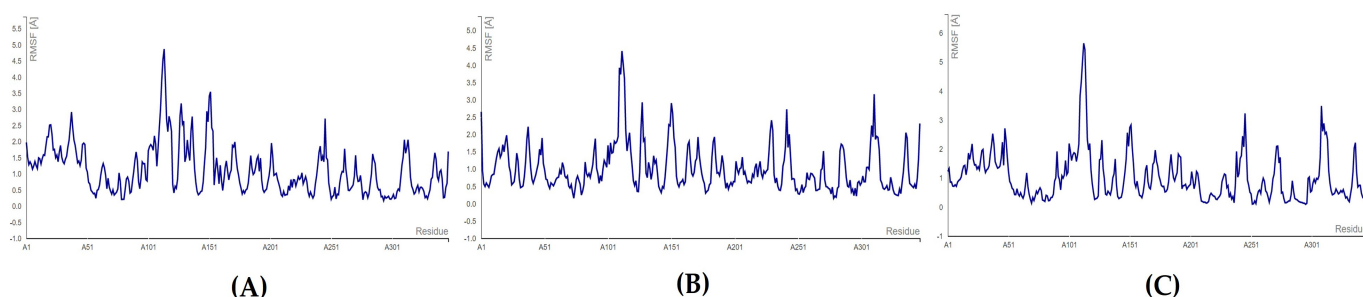


Figure 9. RMSF plots for endoribonuclease protein: (A) nsp15–bromophycoic acid B; (B) nsp15–bromophycoic acid C; (C) nsp15–floridoside.

3.5. Toxicity Evaluation

Using the ProTox-II and StopTox webserver, the toxic characteristics of finalized natural compounds were studied.

3.5.1. ProTox-II Report

The ProTox-II algorithm divides ligands into six toxicity classes based on *LD50* scores, which are estimates of the median lethal dosage, i.e., at which 50% of the test subjects pass away after oral exposure. In addition, the ability to cause genetic abnormalities as well as the danger of liver damage and cancer-causing potential were examined.

As members of class 2 ($5 < LD50 < 50$), thyrserenol A, bromophycoic acids B and C have the potential to be lethal upon oral consumption. The class 4 members included bromophycolide E, H, P, R and S ($300 < LD50 < 2000$). They are not hazardous, but oral consumption might be harmful. Ultimately, floridoside received the class 6 distinction ($LD50 > 5000$), which indicates a likelihood of non-toxicity. It was determined that none of the nine NPs were mutagenic, carcinogenic, or hepatotoxic. Bromophycolides and thyrserenol A, however, may cause immune toxicity (see Table 4).

Table 4. ProTox-II results for shortlisted NPs.

Top Ligands	ProTox-II Toxicity					
	Toxicity Values		Probability			
	LD50 (mg/kg)	Toxicity Class	Hepatotoxicity	Carcinogenicity	Immunotoxicity	Mutagenicity
Bromophycoic acid B	12	2	Inactive	Inactive	Inactive	Inactive
Bromophycoic acid C	12	2	Inactive	Inactive	Inactive	Inactive
Bromophycolide E	1000	4	Inactive	Inactive	Active	Inactive
Bromophycolide H	1000	4	Inactive	Inactive	Active	Inactive
Bromophycolide P	1000	4	Inactive	Inactive	Active	Inactive
Bromophycolide R	1000	4	Inactive	Inactive	Active	Inactive
Bromophycolide S	1000	4	Inactive	Inactive	Active	Inactive
Floridoside	23,000	6	Inactive	Inactive	Inactive	Inactive
Thyrserenol A	7	2	Inactive	Inactive	Active	Inactive

3.5.2. StopTox Report

The StopTox server provided us with estimations of the likelihood that the selected NPs would cause acute toxicity.

Bromophycoic acids, bromophycolide E, H, P and floridoside have been indicated to be non-toxic when inhaled. Nevertheless, bromophycolide R and S could be harmful if inhaled. Bromophycoic acids, bromophycolide E and thyrserenol A were capable of showing the likelihood of oral harm. All nine NPs are unlikely to cause dermal toxicity, eye or skin irritation, or corrosion. Ultimately, the five bromophycolides may cause skin sensitivity (see Table 5).

Table 5. StopTox results for shortlisted NPs.

Top Ligands	StopTox Acute Toxicity				
	Endpoints				
	Inhalation	Oral	Dermal	Irritation and Corrosion	Skin Sensitization
Bromophycoic acid B	Non-Toxic	Toxic	Non-Toxic	Eyes (-) Skin (-)	Non-sensitizer
Bromophycoic acid C	Non-Toxic	Toxic	Non-Toxic	Eyes (-) Skin (-)	Non-sensitizer
Bromophycolide E	Non-Toxic	Toxic	Non-Toxic	Eyes (-) Skin (-)	Sensitizer
Bromophycolide H	Non-Toxic	Non-Toxic	Non-Toxic	Eyes (-) Skin (-)	Sensitizer
Bromophycolide P	Non-Toxic	Non-Toxic	Non-Toxic	Eyes (-) Skin (-)	Sensitizer
Bromophycolide R	Toxic	Non-Toxic	Non-Toxic	Eyes (-) Skin (-)	Sensitizer
Bromophycolide S	Toxic	Non-Toxic	Non-Toxic	Eyes (-) Skin (-)	Sensitizer
Floridoside	Non-Toxic	Non-Toxic	Non-Toxic	Eyes (-) Skin (-)	Non-sensitizer
Thyrsenol A	Non-toxic	Toxic	Non-toxic	Eyes (-) Skin (-)	Non-sensitizer

3.6. Pharmacokinetic Studies

3.6.1. Lipinski Framework (Ro5)

The Lipinski rule of five, commonly referred to as Pfizer's rule, demonstrated the candidate NPs' drug-like potency (see Table 6). With the exception of floridoside, all NPs violated the first criterion ($MW \leq 500$). The criteria of maximum rotatable bonds ($RB \leq 10$) and hydrogen bond acceptors ($HBA \leq 10$) were both followed by all NPs. Only floridoside deviated from the $HBD \leq 5$ limit for maximal hydrogen bond donors. The maximum Consensus log p -value was exceeded by all five bromophycolides ($\log p \leq 5$), whereas floridoside received a negative score. The total number of NPs did not surpass the TPSA's [$(\text{\AA}^2) \leq 140$] upper limit.

Table 6. Results for drug-likeness of the NPs.

Top Ligands	Drug-Likeness Assessment					
	Mol. Weight (g/mol) $MW \leq 500$	Rotatable Bonds $RB \leq 10$	H Bond Acceptors $HBA \leq 10$	H Bond Donors $HBD \leq 5$	C Log p $\log p \leq 5$	TPSA (\AA^2) ≤ 140
Bromophycoic acid B	521.48	5	5	3	4.78	86.99
Bromophycoic acid C	537.48	6	6	3	4.77	96.22
Bromophycolide E	584.38	1	4	2	5.79	66.76
Bromophycolide H	665.29	0	4	2	6.10	66.76
Bromophycolide P	584.38	0	4	1	5.83	55.76
Bromophycolide R	503.47	1	4	1	5.54	59.06
Bromophycolide S	584.38	1	4	1	5.87	59.06
Floridoside	254.23	5	8	6	-2.53	139.84
Thyrsenol A	619.63	8	8	4	3.51	117.84

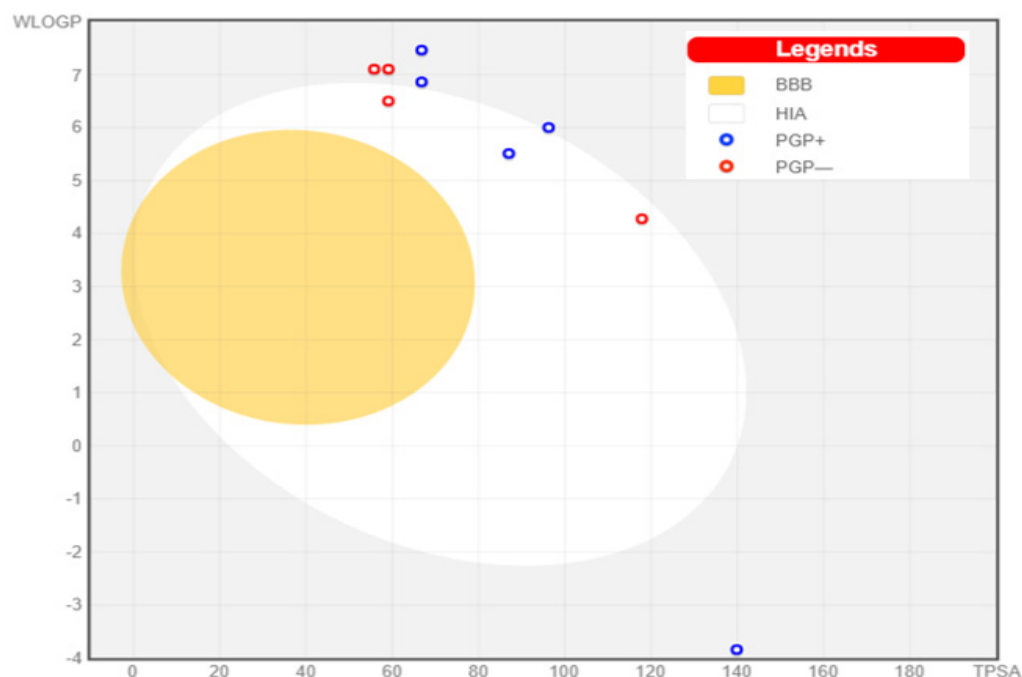
3.6.2. Swiss-ADME

Both bromophycoic acids and thyrsenol A were found to be moderately soluble with the high bioavailability score. All five bromophycolides, on the other hand, were shown to have low water solubility. The bioavailability levels for them were the lowest. Lastly, floridoside has a 0.55 bioavailability value, making it potentially soluble. Just three NPs had a high likelihood of GI absorption; the likelihood was modest for the other five. The bromophycolide P had the greatest AB%, followed by the two bromophycoic acids R and S, with floridoside having the lowest (see Table 7).

Table 7. Results for Swiss-ADME analysis.

Swiss-ADME Output					
Top Ligands	Water Solubility	Bioavailability	GI Absorption	Absorption (%)	BBB Permeant
Bromophycoic acid B	Moderate	0.56	High	78.98	No
Bromophycoic acid C	Moderate	0.56	Low	75.80	No
Bromophycolide E	Poor	0.17	Low	85.96	No
Bromophycolide H	Poor	0.17	Low	85.96	No
Bromophycolide P	Poor	0.17	Low	89.76	No
Bromophycolide R	Poor	0.17	High	88.62	No
Bromophycolide S	Poor	0.17	Low	88.62	No
Floridoside	Soluble	0.55	Low	60.75	No
Thyrsenol A	Moderate	0.55	High	68.34	No

The GI tract was predicted not to be able to passively absorb six NPs, namely, bromophycoic acid C, bromophycolide E, H, P, and S. On the other hand, the GI tract may passively absorb bromophycoic acid B, bromophycolide R, and thyrsenol A. The blood–brain barrier was impermeable to all of the NPs of interest (see Figure 10).

**Figure 10.** Boiled egg graph for the nine NPs.

3.6.3. Bioactivity Evaluation

One of the most important steps in the pre-clinical drug-screening process is the assessment of bioactivity. The following NPs' probable bioactivity was predicted by the PASS online program.

According to predictions, all NPs are potential antifungals that might aid in treating fungal infections linked to COVID-19. Antifungal qualities such as 1, 3-Beta-glucan synthase, beta glucuronidase, histidine kinase, rhizopuspepsin, and GRP78 expression inhibitors were linked to potential inhibition of COVID-19-associated mucormycosis (CAM) [204]. As possible histidine kinase inhibitors, bromophycoic acid B, bromophycolide E, H, P, R, and, S may block the important functional residues of Nsp15 protein, such as HIS: 234, 235, 242, 249, and 250. Four NPs, namely, bromophycoic acid C, the three bromophycolides, floridoside, and thyrsenol A were anticipated to have antiviral properties, indicating a higher likelihood of inhibiting the viral target—in this case, SARS-

CoV-2. Depending on the stage of infection, additional relevant bioactivities may help to mitigate the effects of SARS-CoV-2 by either directly or indirectly influencing the immune system, including interferon antagonist, interferon gamma antagonist, transcription factor NF kappa B stimulant or inhibitor, immunostimulant, immunosuppressant, interleukin agonist and antagonist, cytokine release inhibitor, TNF expression, and JAK2 expression inhibitor [205,206]. It is interesting to note that floridoside was predicted to be effective in treating severe acute respiratory syndrome (see Table 8).

Table 8. Potential bioactivity for selected NPs.

PASS Online Program	
Top Ligands	Potential Bioactivity
Bromophycoic acid B	Antifungal, Histidine kinase inhibitor, Beta glucuronidase inhibitor, Antibacterial, Antioxidant, Antineoplastic, Interferon antagonist, Interferon gamma antagonist, Transcription factor NF kappa B stimulant, Immunostimulant
Bromophycoic acid C	Antifungal, Antiviral, Antioxidant, Anticancer, Antineoplastic, Beta glucuronidase inhibitor, Transcription factor NF kappa B stimulant
Bromophycolide E	Antineoplastic, Antibiotic, Antiviral, Antifungal, Beta glucuronidase inhibitor, Histidine kinase inhibitor, MMP9 expression inhibitor, Immunosuppressant, Respiratory analeptic, Antibacterial, Cytokine release inhibitor, Interleukin 10 antagonist, 1,3-Beta-glucan synthase inhibitor, Interferon gamma antagonist
Bromophycolide H	Antineoplastic, MMP9 expression inhibitor, Antifungal, Antibacterial, Antibiotic, Histidine kinase inhibitor, Cytokine release inhibitor, Interferon gamma antagonist, Interleukin 10 antagonist, 1,3-Beta-glucan synthase inhibitor
Bromophycolide P	Antineoplastic, Respiratory analeptic, Antibacterial, Antibiotic, Antifungal, MMP9 expression inhibitor, Beta glucuronidase inhibitor, Histidine kinase inhibitor, 1,3-Beta-glucan synthase inhibitor, Immunosuppressant, Interferon gamma antagonist, Cytokine release inhibitor, Expectorant,
Bromophycolide R	Antiviral, Antineoplastic alkaloid, Anticancer, Antifungal, Antibiotic, Antibacterial, Immunosuppressant, Transcription factor NF kappa B stimulant, Beta glucuronidase inhibitor, Histidine kinase inhibitor, 1,3-Beta-glucan synthase inhibitor, Respiratory analeptic, Anti-inflammatory, Cytokine release inhibitor, Interferon gamma antagonist, and an Interleukin 10 antagonist.
Bromophycolide S	Antiviral, Antineoplastic, Antibiotic, Anticancer, Antifungal, Immunosuppressant, Antibacterial, Transcription factor NF kappa B inhibitor, Histidine kinase inhibitor, Beta glucuronidase inhibitor, 1,3-Beta-glucan synthase inhibitor, Cytokine release inhibitor and an Interleukin 10 antagonist.
Floridoside	Antiviral, Anti-parasitic, Antifungal, Antifungal enhancer, Antibacterial, Anti-tuberculosic, Anticancer, Anti-infective, Antioxidant, Free radical scavenger, Anti-diabetic, Antineoplastic, Immunostimulant, Immunomodulator, Macrophage stimulant, Macrophage colony stimulating factor agonist, Respiratory analeptic, Transcription factor NF kappa B stimulant, Histamine release stimulant, Beta glucuronidase inhibitor, 1,3-Beta-glucan synthase inhibitor, Rhizopuspepsin inhibitor, GRP78 expression inhibitor, Mucolytic, Expectorant, Anti-inflammatory, Histamine release inhibitor, JAK2 expression inhibitor, Severe acute respiratory syndrome treatment, RdRp Inhibitor, Interferon gamma antagonist, Respiratory distress syndrome treatment, Cytokine release inhibitor, TNF expression inhibitor, Interleukin 2, 10, 12 agonist, Interleukin 1a, 4, 6 antagonist.
Thyrsenol A	Antineoplastic, Antifungal, Antiviral, Antiinflammatory, Antibacterial, Antibiotic

4. Conclusions

In conclusion, in this work, we conducted in silico trials on natural compounds from the *Laurencia* genus to find potential candidates for the treatment of SARS-CoV-2's RdRp and nsp15 enzymatic infections. Our research identified promising *Laurencia* red algal anti-SARS-CoV-2 products. The final seven candidates that were shortlisted for RdRp unmistakably exhibit strong interactions with the relevant residues that are crucial for the enzyme inhibition. Three of the seven ligands have the potential to inhibit RdRp when they bind to the N-terminal (AS2), whereas the remaining four ligands are effective RdRp inhibitors when they attach to the NTP entry channel at the C-terminal (AS1). Bromophycolide R displayed the best interaction with the β -hairpin motif region of RdRp (AS2). On the other hand, bromophycolide E and thyrsenol A demonstrated the most favorable residue interactions in the C-terminal (AS1) of RNA-dependent RNA polymerase. As a result of the correlation and required synergy (allosteric signaling) between the two active sites, the RdRp will ultimately be inhibited in both scenarios. The critical residues of nsp15 were interacted with best by bromophycoic acid B, C, and floridoside. Bromophycoic acid C had highly favorable amino acid interactions with both RdRp (N-terminal) and nsp15 proteins, making it a likely dual target inhibitor. Given the nature of the identified amino

acid interactions, we propose additional research into the thyrsenol B, dehydrothyrsiferol, and thyrsiferol, against RdRp and nsp15 proteins. To increase the therapeutic prospects of these NPs, laboratory modifications are suggested by assessments of their toxicity and pharmacokinetics analyses.

Supplementary Materials: The following supporting information can be downloaded at: <https://www.mdpi.com/article/10.3390/microbiolres14030069/s1>, Table S1: A list of 300 natural products from the red algal Genus *Laurencia* involved in this work; Table S2: Natural products listed under subcategory 1 in low class for RdRp; Table S3: Natural products listed under subcategory 2 in low class for RdRp; Table S4: Natural products listed in lower-moderate class for RdRp; Table S5: Natural products listed in upper-moderate class for RdRp; Table S6: Natural products with highest binding affinity for RdRp; Table S7: Outcome of docking the C-terminal catalytic region of RdRp; Table S8: Natural products listed under subcategory 1 in low class for nsp15; Table S9: Natural products listed under sub-category 2 in low class for nsp15; Table S10: Natural products listed in lower-moderate class for nsp15; Table S11: Natural products listed in upper-moderate class for nsp15; Table S12: Natural products with highest binding affinity for nsp15; Table S13: MD Simulations for N-Terminal docked complexes; Table S14: MD Simulations for C-Terminal docked complexes; Table S15: MD Simulations for nsp15 docked complexes; Table S16: SMILES line notations for selected NPs.

Author Contributions: Conceptualization, O.P. and G.V.Z.; methodology, O.P.; software, O.P.; formal analysis, O.P.; investigation, O.P.; data curation, O.P. and H.A.; writing—original draft preparation, O.P.; writing—review and editing, O.P., H.A., G.V.Z. and M.V.T. supervision, G.V.Z. and M.V.T. All authors have read and agreed to the published version of the manuscript.

Funding: This research was funded by the Ministry of Science and Higher Education of the Russian Federation (Reference # 075-15-2022-1118, dated 29 June 2022).

Institutional Review Board Statement: Not applicable.

Informed Consent Statement: Not applicable.

Data Availability Statement: Not applicable.

Conflicts of Interest: Authors declare no conflict of interest.

References

1. Lopez Bernal, J.; Andrews, N.; Gower, C.; Gallagher, E.; Simmons, R.; Thelwall, S.; Stowe, J.; Tessier, E.; Groves, N.; Dabrera, G.; et al. Effectiveness of COVID-19 Vaccines against the B.1.617.2 (Delta) Variant. *N. Engl. J. Med.* **2021**, *385*, 585–594. [\[CrossRef\]](#) [\[PubMed\]](#)
2. Puranik, A.; Lenehan, P.J.; Silvert, E.; Niesen, M.J.M.; Corchado-Garcia, J.; O'horo, J.C.; Virk, A.; Swift, M.D.; Halamka, J.; Badley, A.D.; et al. Comparison of two highly-effective mRNA vaccines for COVID-19 during periods of Alpha and Delta variant prevalence. *medRxiv*, 2021; preprint. [\[CrossRef\]](#)
3. Callaway, E. COVID drug drives viral mutations—And now some want to halt its use. *Nature* **2023**, *614*, 399. [\[CrossRef\]](#)
4. Phillips, N. The coronavirus is here to stay—here's what that means. *Nature* **2021**, *590*, 382–384. [\[CrossRef\]](#)
5. Min, J.S.; Kwon, S.; Jin, Y.-H. SARS-CoV-2 RdRp Inhibitors Selected from a Cell-Based SARS-CoV-2 RdRp Activity Assay System. *Biomedicines* **2021**, *9*, 996. [\[CrossRef\]](#)
6. Ahn, D.-G.; Choi, J.-K.; Taylor, D.R.; Oh, J.-W. Biochemical characterization of a recombinant SARS coronavirus nsp12 RNA-dependent RNA polymerase capable of copying viral RNA templates. *Arch. Virol.* **2012**, *157*, 2095–2104. [\[CrossRef\]](#)
7. De Farias, S.T.; Dos Santos, A.P.D.S., Jr.; Rêgo, T.G.D.; José, M.V. Origin and Evolution of RNA-Dependent RNA Polymerase. *Front. Genet.* **2017**, *8*, 125. [\[CrossRef\]](#) [\[PubMed\]](#)
8. Beigel, J.H.; Tomashek, K.M.; Dodd, L.E.; Mehta, A.K.; Zingman, B.S.; Kalil, A.C.; Hohmann, E.; Chu, H.Y.; Luetkemeyer, A.; Kline, S.; et al. Remdesivir for the Treatment of COVID-19—Final Report. *N. Engl. J. Med.* **2020**, *383*, 1813–1826. [\[CrossRef\]](#)
9. Jockusch, S.; Tao, C.; Li, X.; Chien, M.; Kumar, S.; Morozova, I.; Kalachikov, S.; Russo, J.J.; Ju, J. Sofosbuvir terminated RNA is more resistant to SARS-CoV-2 proofreader than RNA terminated by Remdesivir. *Sci. Rep.* **2020**, *10*, 16577. [\[CrossRef\]](#)
10. Chien, M.; Anderson, T.K.; Jockusch, S.; Tao, C.; Li, X.; Kumar, S.; Russo, J.J.; Kirchdoerfer, R.N.; Ju, J. Nucleotide Analogues as Inhibitors of SARS-CoV-2 Polymerase, a Key Drug Target for COVID-19. *J. Proteome Res.* **2020**, *19*, 4690–4697. [\[CrossRef\]](#)
11. Ju, J.; Li, X.; Kumar, S.; Jockusch, S.; Chien, M.; Tao, C.; Morozova, I.; Kalachikov, S.; Kirchdoerfer, R.N.; Russo, J.J. Nucleotide analogues as inhibitors of SARS-CoV Polymerase. *Pharmacol. Res. Perspect.* **2020**, *8*, e00674. [\[CrossRef\]](#) [\[PubMed\]](#)
12. Aftab, S.O.; Ghouri, M.Z.; Masood, M.U.; Haider, Z.; Khan, Z.; Ahmad, A.; Munawar, N. Analysis of SARS-CoV-2 RNA-dependent RNA polymerase as a potential therapeutic drug target using a computational approach. *J. Transl. Med.* **2020**, *18*, 275. [\[CrossRef\]](#)

13. Ahmad, J.; Ikram, S.; Ahmad, F.; Rehman, I.U.; Mushtaq, M. SARS-CoV-2 RNA Dependent RNA polymerase (RdRp)—A drug repurposing study. *Heliyon* **2020**, *6*, e04502. [\[CrossRef\]](#)
14. Aktaş, A.; Tüzün, B.; Aslan, R.; Sayin, K.; Ataseven, H. New anti-viral drugs for the treatment of COVID-19 instead of favipiravir. *J. Biomol. Struct. Dyn.* **2020**, *39*, 7263–7273. [\[CrossRef\]](#)
15. Alexpandi, R.; De Mesquita, J.F.; Pandian, S.K.; Ravi, A.V. Quinolines-Based SARS-CoV-2 3CLpro and RdRp Inhibitors and Spike-RBD-ACE2 Inhibitor for Drug-Repurposing Against COVID-19: An in silico Analysis. *Front. Microbiol.* **2020**, *11*, 1796. [\[CrossRef\]](#) [\[PubMed\]](#)
16. Al-Masoudi, N.A.; Elias, R.S.; Saeed, B. Molecular Docking Studies of some Antiviral and Antimalarial Drugs Via Bindings to 3CL-Protease and Polymerase Enzymes of the Novel Coronavirus (SARS-CoV-2). *Biointerface Res. Appl. Chem.* **2020**, *10*, 6444–6459. [\[CrossRef\]](#)
17. Ao, S.; Han, D.; Sun, L.; Wu, Y.; Liu, S.; Huang, Y. Identification of Potential Key Agents for Targeting RNA-Dependent RNA Polymerase of SARS-CoV-2 by Integrated Analysis and Virtual Drug Screening. *Front. Genet.* **2020**, *11*, 581668. [\[CrossRef\]](#) [\[PubMed\]](#)
18. Calligari, P.; Bobone, S.; Ricci, G.; Bocedi, A. Molecular Investigation of SARS-CoV-2 Proteins and Their Interactions with Antiviral Drugs. *Viruses* **2020**, *12*, 445. [\[CrossRef\]](#)
19. Da Silva, F.M.A.; Da Silva, K.P.A.; De Oliveira, L.P.M.; Costa, E.V.; Koolen, H.H.; Pinheiro, M.L.B.; De Souza, A.Q.L.; De Souza, A.D.L. Flavonoid glycosides and their putative human metabolites as potential inhibitors of the SARS-CoV-2 main protease (Mpro) and RNA-dependent RNA polymerase (RdRp). *Mem. Instit. Oswaldo Cruz.* **2020**, *115*, e200207. [\[CrossRef\]](#)
20. da Silva, J.K.R.; Figueiredo, P.L.B.; Byler, K.G.; Setzer, W.N. Essential Oils as Antiviral Agents, Potential of Essential Oils to Treat SARS-CoV-2 Infection: An In-Silico Investigation. *Int. J. Mol. Sci.* **2020**, *21*, 3426. [\[CrossRef\]](#)
21. Elfiky, A.A. Anti-HCV, nucleotide inhibitors, repurposing against COVID-19. *Life Sci.* **2020**, *248*, 117477. [\[CrossRef\]](#) [\[PubMed\]](#)
22. Elfiky, A.A. SARS-CoV-2 RNA dependent RNA polymerase (RdRp) targeting: An in silico perspective. *J. Biomol. Struct. Dyn.* **2021**, *39*, 3204–3212. [\[CrossRef\]](#) [\[PubMed\]](#)
23. Indu, P.; Rameshkumar, M.R.; Arunagirinathan, N.; Al-Dhabi, N.A.; Arasu, M.V.; Ignacimuthu, S. Raltegravir, Indinavir, Tipranavir, Dolutegravir, and Etravirine against main protease and RNA-dependent RNA polymerase of SARS-CoV-2: A molecular docking and drug repurposing approach. *J. Infect. Public. Health* **2020**, *13*, 1856–1861. [\[CrossRef\]](#) [\[PubMed\]](#)
24. Kandeel, M.; Kitade, Y.; Almubarak, A. Repurposing FDA-approved phytomedicines, natural products, antivirals and cell protectives against SARS-CoV-2 (COVID-19) RNA-dependent RNA polymerase. *PeerJ* **2020**, *8*, e10480. [\[CrossRef\]](#)
25. Mohamed, T.A.; Elshamy, A.I.; Ibrahim, M.A.A.; Zellagui, A.; Moustafa, M.F.; Abdelrahman, A.H.M.; Ohta, S.; Pare, P.W.; Hegazy, M.-E.F. Carotane sesquiterpenes from *Ferula vesceritensis*: In silico analysis as SARS-CoV-2 binding inhibitors. *RSC Adv.* **2020**, *10*, 34541–34548. [\[CrossRef\]](#)
26. Parvez, M.S.A.; Karim, M.A.; Hasan, M.; Jaman, J.; Karim, Z.; Tahsin, T.; Hasan, M.N.; Hosen, M.J. Prediction of potential inhibitors for RNA-dependent RNA polymerase of SARS-CoV-2 using comprehensive drug repurposing and molecular docking approach. *Int. J. Biol. Macromol.* **2020**, *163*, 1787–1797. [\[CrossRef\]](#)
27. Pokhrel, R.; Chapagain, P.; Siltberg-Liberles, J. Potential RNA-dependent RNA polymerase inhibitors as prospective therapeutics against SARS-CoV-2. *J. Med. Microbiol.* **2020**, *69*, 864–873. [\[CrossRef\]](#)
28. Ruan, Z.; Liu, C.; Guo, Y.; He, Z.; Huang, X.; Jia, X.; Yang, T. SARS-CoV-2 and SARS-CoV: Virtual screening of potential inhibitors targeting RNA-dependent RNA polymerase activity (NSP12). *J. Med. Virol.* **2021**, *93*, 389–400. [\[CrossRef\]](#)
29. Tchesnokov, E.P.; Gordon, C.J.; Woolner, E.; Kocinkova, D.; Perry, J.K.; Feng, J.Y.; Porter, D.P.; Götte, M. Template-dependent inhibition of coronavirus RNA-dependent RNA polymerase by remdesivir reveals a second mechanism of action. *J. Biol. Chem.* **2020**, *295*, 16156. [\[CrossRef\]](#)
30. Wu, C.; Liu, Y.; Yang, Y.; Zhang, P.; Zhong, W.; Wang, Y.; Wang, Q.; Xu, Y.; Li, M.; Li, X.; et al. Analysis of therapeutic targets for SARS-CoV-2 and discovery of potential drugs by computational methods. *Acta Pharm. Sin. B* **2020**, *10*, 766–788. [\[CrossRef\]](#)
31. Ahmed, S.; Mahtarin, R.; Ahmed, S.S.; Akter, S.; Islam, S.; Al Mamun, A.; Islam, R.; Hossain, N.; Ali, A.; Sultana, M.U.C.; et al. Investigating the binding affinity, interaction, and structure-activity-relationship of 76 prescription antiviral drugs targeting RdRp and Mpro of SARS-CoV-2. *J. Biomol. Struct. Dyn.* **2021**, *39*, 6290–6305. [\[CrossRef\]](#) [\[PubMed\]](#)
32. Barage, S.; Karthic, A.; Bavi, R.; Desai, N.; Kumar, R.; Kumar, V.; Lee, K.W. Identification and characterization of novel RdRp and Nsp15 inhibitors for SARS-COV2 using computational approach. *J. Biomol. Struct. Dyn.* **2022**, *40*, 2557–2574. [\[CrossRef\]](#) [\[PubMed\]](#)
33. Borquaye, L.S.; Gasu, E.N.; Ampomah, G.B.; Kyei, L.K.; Amarh, M.A.; Mensah, C.N.; Nartey, D.; Commodore, M.; Adomako, A.K.; Acheampong, P.; et al. Alkaloids from *Cryptolepis sanguinolenta* as Potential Inhibitors of SARS-CoV-2 Viral Proteins: An In Silico Study. *BioMed Res. Int.* **2020**, *2020*, 532–560. [\[CrossRef\]](#) [\[PubMed\]](#)
34. Dwarka, D.; Agoni, C.; Mellem, J.J.; Soliman, M.E.; Baijnath, H. Identification of potential SARS-CoV-2 inhibitors from South African medicinal plant extracts using molecular modelling approaches. *S. Afr. J. Bot.* **2020**, *133*, 273–284. [\[CrossRef\]](#) [\[PubMed\]](#)
35. El Hassab, M.A.; Shoun, A.A.; Al-Rashood, S.T.; Al-Warhi, T.; Eldehna, W.M. Identification of a New Potential SARS-COV-2 RNA-Dependent RNA Polymerase Inhibitor via Combining Fragment-Based Drug Design, Docking, Molecular Dynamics, and MM-PBSA Calculations. *Front. Chem.* **2020**, *8*, 584894. [\[CrossRef\]](#) [\[PubMed\]](#)
36. Gul, S.; Ozcan, O.; Asar, S.; Okyar, A.; Baris, I.; Kavakli, I.H. In silico identification of widely used and well-tolerated drugs as potential SARS-CoV-2 3C-like protease and viral RNA-dependent RNA polymerase inhibitors for direct use in clinical trials. *J. Biomol. Struct. Dyn.* **2021**, *39*, 6772–6791. [\[CrossRef\]](#)

37. Gutierrez-Villagomez, J.M.; Campos-García, T.; Molina-Torres, J.; López, M.G.; Vázquez-Martínez, J. Alkamides and Piperamides as Potential Antivirals against the Severe Acute Respiratory Syndrome Coronavirus 2 (SARS-CoV-2). *J. Phys. Chem. Lett.* **2020**, *11*, 8008–8016. [\[CrossRef\]](#)
38. Kar, P.; Sharma, N.R.; Singh, B.; Sen, A.; Roy, A. Natural compounds from *Clerodendrum* spp. as possible therapeutic candidates against SARS-CoV-2: An in silico investigation. *J. Biomol. Struct. Dyn.* **2021**, *39*, 4774–4785. [\[CrossRef\]](#)
39. Khan, A.; Khan, M.; Saleem, S.; Babar, Z.; Ali, A.; Khan, A.A.; Sardar, Z.; Hamayun, F.; Ali, S.S.; Wei, D.-Q. Phylogenetic Analysis and Structural Perspectives of RNA-Dependent RNA-Polymerase Inhibition from SARs-CoV-2 with Natural Products. *Interdiscip. Sci. Comput. Life Sci.* **2020**, *12*, 335–348. [\[CrossRef\]](#)
40. Mutlu, O.; Ugurel, O.M.; Sariyer, E.; Ata, O.; Inci, T.G.; Ugurel, E.; Kocer, S.; Turgut-Balik, D. Targeting SARS-CoV-2 Nsp12/Nsp8 interaction interface with approved and investigational drugs: An in silico structure-based approach. *J. Biomol. Struct. Dyn.* **2022**, *40*, 918–930. [\[CrossRef\]](#)
41. Narayanan, N.; Nair, D.T. Vitamin B12 may inhibit RNA-dependent-RNA polymerase activity of nsp12 from the SARS-CoV-2 virus. *IUBMB Life* **2020**, *72*, 2112–2120. [\[CrossRef\]](#)
42. Ribaudo, G.; Ongaro, A.; Oselladore, E.; Zagotto, G.; Memo, M.; Gianoncelli, A. A computational approach to drug repurposing against SARS-CoV-2 RNA dependent RNA polymerase (RdRp). *J. Biomol. Struct. Dyn.* **2022**, *40*, 1101–1108. [\[CrossRef\]](#) [\[PubMed\]](#)
43. Sharma, A.; Vora, J.; Patel, D.; Sinha, S.; Jha, P.C.; Shrivastava, N. Identification of natural inhibitors against prime targets of SARS-CoV-2 using molecular docking, molecular dynamics simulation and MM-PBSA approaches. *J. Biomol. Struct. Dyn.* **2022**, *40*, 3296–3311. [\[CrossRef\]](#)
44. Singh, J.; Malik, D.; Raina, A. Computational investigation for identification of potential phytochemicals and antiviral drugs as potential inhibitors for RNA-dependent RNA polymerase of COVID-19. *J. Biomol. Struct. Dyn.* **2022**, *40*, 3492–3507. [\[CrossRef\]](#) [\[PubMed\]](#)
45. Singh, S.; Sk, M.F.; Sonawane, A.; Kar, P.; Sadhukhan, S. Plant-derived natural polyphenols as potential antiviral drugs against SARS-CoV-2 via RNA-dependent RNA polymerase (RdRp) inhibition: An in-silico analysis. *J. Biomol. Struct. Dyn.* **2021**, *39*, 6249–6264. [\[CrossRef\]](#) [\[PubMed\]](#)
46. Elkarhat, Z.; Charoute, H.; Elkhatabi, L.; Barakat, A.; Rouba, H. Potential inhibitors of SARS-CoV-2 RNA dependent RNA polymerase protein: Molecular docking, molecular dynamics simulations and MM-PBSA analyses. *J. Biomol. Struct. Dyn.* **2022**, *40*, 361–374. [\[CrossRef\]](#) [\[PubMed\]](#)
47. Brunt, D.; Lakernick, P.M.; Wu, C. Discovering new potential inhibitors to SARS-CoV-2 RNA dependent RNA polymerase (RdRp) using high throughput virtual screening and molecular dynamics simulations. *Sci. Rep.* **2022**, *12*, 19986. [\[CrossRef\]](#)
48. Olender, S.A.; Perez, K.K.; Go, A.S.; Balani, B.; Price-Haywood, E.G.; Shah, N.S.; Wang, S.; Walunas, T.L.; Swaminathan, S.; Slim, J.; et al. Remdesivir for Severe Coronavirus Disease 2019 (COVID-19) Versus a Cohort Receiving Standard of Care. *Clin. Infect. Dis.* **2021**, *73*, e4166–e4174. [\[CrossRef\]](#) [\[PubMed\]](#)
49. Al-Abdouh, A.; Bizanti, A.; Barbarawi, M.; Jabri, A.; Kumar, A.; Fashanu, O.E.; Khan, S.U.; Zhao, D.; Antar, A.A.; Michos, E.D. Remdesivir for the treatment of COVID-19: A systematic review and meta-analysis of randomized controlled trials. *Contemp. Clin. Trials* **2021**, *101*, 106272. [\[CrossRef\]](#)
50. Dölken, L.; Stich, A.; Spinner, C.D. Remdesivir for Early COVID-19 Treatment of High-Risk Individuals Prior to or at Early Disease Onset—Lessons Learned. *Viruses* **2021**, *13*, 963. [\[CrossRef\]](#)
51. Gottlieb, R.L.; Vaca, C.E.; Paredes, R.; Mera, J.; Webb, B.J.; Perez, G.; Oguchi, G.; Ryan, P.; Nielsen, B.U.; Brown, M.; et al. Early Remdesivir to Prevent Progression to Severe COVID-19 in Outpatients. *N. Engl. J. Med.* **2022**, *386*, 305–315. [\[CrossRef\]](#)
52. Mahajan, L.; Singh, A. Gifty Clinical outcomes of using remdesivir in patients with moderate to severe COVID-19: A prospective randomised study. *Indian J. Anaesth.* **2021**, *65* (Suppl. 1), S41–S46. [\[CrossRef\]](#) [\[PubMed\]](#)
53. Russo, A.; Binetti, E.; Borrazzo, C.; Cacciola, E.G.; Battistini, L.; Ceccarelli, G.; Mastroianni, C.M.; D’ettorre, G. Efficacy of Remdesivir-Containing Therapy in Hospitalized COVID-19 Patients: A Prospective Clinical Experience. *J. Clin. Med.* **2021**, *10*, 3784. [\[CrossRef\]](#) [\[PubMed\]](#)
54. Yan, V.C.; Muller, F.L. Why Remdesivir Failed: Preclinical Assumptions Overestimate the Clinical Efficacy of Remdesivir for COVID-19 and Ebola. *Antimicrob. Agents Chemother.* **2021**, *65*, e0111721. [\[CrossRef\]](#) [\[PubMed\]](#)
55. Ader, F.; Bouscambert-Duchamp, M.; Hites, M.; Peiffer-Smadja, N.; Poissy, J.; Belhadi, D.; Diallo, A.; Lê, M.-P.; Peytavin, G.; Staub, T.; et al. Remdesivir plus standard of care versus standard of care alone for the treatment of patients admitted to hospital with COVID-19 (DisCoVeRy): A phase 3, randomised, controlled, open-label trial. *Lancet Infect. Dis.* **2022**, *22*, 209–221. [\[CrossRef\]](#)
56. Sun, D. Remdesivir for Treatment of COVID-19: Combination of Pulmonary and IV Administration May Offer Additional Benefit. *AAPS J.* **2020**, *22*, 77, Erratum in *AAPS J.* **2020**, *22*, 102. [\[CrossRef\]](#)
57. Martínez, D.R.; Schäfer, A.; Leist, S.R.; Li, D.; Gully, K.; Yount, B.; Feng, J.Y.; Bunyan, E.; Porter, D.P.; Cihlar, T.; et al. Prevention and therapy of SARS-CoV-2 and the B.1.351 variant in mice. *Cell Rep.* **2021**, *36*, 109450. [\[CrossRef\]](#)
58. Taha, H.R.; Keewan, N.; Slati, F.; Al-Sawalha, N.A. Remdesivir: A Closer Look at Its Effect in COVID-19 Pandemic. *Pharmacology* **2021**, *106*, 462–468. [\[CrossRef\]](#)
59. Matsuyama, S.; Kawase, M.; Nao, N.; Shirato, K.; Ujike, M.; Kamitani, W.; Shimojima, M.; Fukushi, S. The Inhaled Steroid Ciclesonide Blocks SARS-CoV-2 RNA Replication by Targeting the Viral Replication-Transcription Complex in Cultured Cells. *J. Virol.* **2020**, *95*, e01648-20. [\[CrossRef\]](#)

60. Yang, J.-W.; Fan, L.-C.; Miao, X.-Y.; Mao, B.; Li, M.-H.; Lu, H.-W.; Liang, S.; Xu, J.-F. Corticosteroids for the treatment of human infection with influenza virus: A systematic review and meta-analysis. *Clin. Microbiol. Infect.* **2015**, *21*, 956–963. [\[CrossRef\]](#)
61. Kim, Y.; Jedrzejczak, R.; Maltseva, N.I.; Wilamowski, M.; Endres, M.; Godzik, A.; Michalska, K.; Joachimiak, A. Crystal structure of Nsp15 endoribonuclease NendoU from SARS-CoV-2. *Protein Sci.* **2020**, *29*, 1596–1605. [\[CrossRef\]](#) [\[PubMed\]](#)
62. Liu, X.; Fang, P.; Fang, L.; Hong, Y.; Zhu, X.; Wang, D.; Peng, G.; Xiao, S. Porcine deltacoronavirus nsp15 antagonizes interferon- β production independently of its endoribonuclease activity. *Mol. Immunol.* **2019**, *114*, 100–107. [\[CrossRef\]](#)
63. El Sayed, K.A. Natural Products as Antiviral Agents. *Stud. Nat. Prod. Chem.* **2000**, *24*, 473–572. [\[CrossRef\]](#)
64. Bzówka, M.; Mitusińska, K.; Raczynska, A.; Samol, A.; Tuszyński, J.A.; Góra, A. Structural and Evolutionary Analysis Indicate That the SARS-CoV-2 Mpro Is a Challenging Target for Small-Molecule Inhibitor Design. *Int. J. Mol. Sci.* **2020**, *21*, 3099. [\[CrossRef\]](#)
65. Kolarič, A.; Jukič, M.; Bren, U. Novel Small-Molecule Inhibitors of the SARS-CoV-2 Spike Protein Binding to Neuropilin 1. *Pharmaceuticals* **2022**, *15*, 165. [\[CrossRef\]](#)
66. Yang, L.; Wang, Z. Natural Products, Alone or in Combination with FDA-Approved Drugs, to Treat COVID-19 and Lung Cancer. *Biomedicines* **2021**, *9*, 689. [\[CrossRef\]](#)
67. Wang, Z.; Wang, N.; Yang, L.; Song, X.-Q. Bioactive natural products in COVID-19 therapy. *Front. Pharmacol.* **2022**, *13*, 926507. [\[CrossRef\]](#)
68. Pokharkar, O.; Lakshmanan, H.; Zyryanov, G.V.; Tsurkan, M.V. Antiviral Potential of *Antillogorgia americana* and *elisabethae* Natural Products against nsp16–nsp10 Complex, nsp13, and nsp14 Proteins of SARS-CoV-2: An In Silico Investigation. *Microbiol. Res.* **2023**, *14*, 993–1019.
69. Wang, D.; Huang, J.; Yeung, A.W.K.; Tzvetkov, N.T.; Horbańczuk, J.O.; Willschke, H.; Gai, Z.; Atanasov, A.G. The Significance of Natural Product Derivatives and Traditional Medicine for COVID-19. *Processes* **2020**, *8*, 937. [\[CrossRef\]](#)
70. Ismail, M.M.; Alotaibi, B.S.; El-Sheekh, M.M. Therapeutic Uses of Red Macroalgae. *Molecules* **2020**, *25*, 4411. [\[CrossRef\]](#) [\[PubMed\]](#)
71. Reis, J.G.; Cadamuro, R.D.; Cabral, A.C.; Thaís da Silva, I.T.; Rodríguez-Lázaro, D.; Fongaro, G. Broad Spectrum Algae Compounds Against Viruses. *Front. Microbiol.* **2022**, *12*, 809296. [\[CrossRef\]](#) [\[PubMed\]](#)
72. Pérez-Riverol, A.; Piñón, R.A.; Morier, D.L.F.; Torres, L.Y.; Mendoza, L.D.; Barrio, A.G. Antiviral activity of an aqueous extract from the red alga *Laurencia obtusa* against influenza A and B viruses. *Rev. Cub. Med. Trop.* **2014**, *66*, 273–285.
73. Gheda, S.F.; El-Adawi, H.I.; El-Deeb, N.M. Antiviral Profile of Brown and Red Seaweed Polysaccharides Against Hepatitis C Virus. *Iran. J. Pharm. Res. IJPR* **2016**, *15*, 483–491.
74. Yu, X.-Q.; Jiang, C.-S.; Zhang, Y.; Sun, P.; Kurtán, T.; Mándi, A.; Li, X.-L.; Yao, L.-G.; Liu, A.-H.; Wang, B.; et al. Compositacins A–K: Bioactive chamigrane-type halosquiterpenoids from the red alga *Laurencia composita* Yamada. *Phytochemistry* **2017**, *136*, 81–93. [\[CrossRef\]](#) [\[PubMed\]](#)
75. Lee, S.; Hoshino, M.; Fujita, M.; Urban, S. Cycloelatanene A and B: Absolute configuration determination and structural revision by the crystalline sponge method. *Chem. Sci.* **2017**, *8*, 1547–1550. [\[CrossRef\]](#)
76. Shaaban, M.; Abou-El-Wafa, G.S.E.; Golz, C.; Laatsch, H. New Haloterpenes from the Marine Red Alga *Laurencia papillosa*: Structure Elucidation and Biological Activity. *Mar. Drugs* **2021**, *19*, 35. [\[CrossRef\]](#)
77. Masuda, M.; Kogame, K.; Arisawa, S.; Suzuki, M. Morphology and Halogenated Secondary Metabolites of Three Gran Canaria Species of *Laurencia* (Ceramiales, Rhodophyta). *Bot. Mar.* **1998**, *41*, 265–277. [\[CrossRef\]](#)
78. Senties, A.; Díaz-Larrea, J.; Cassano, V.; Gil-Rodríguez, M.C.; Fujii, M.T. *Laurencia marilzae* (Ceramiales, Rhodophyta) from the Mexican Caribbean: A New Record for the Tropical Western Atlantic. *Bull. Mar. Sci.* **2011**, *87*, 681–686. [\[CrossRef\]](#)
79. Suzuki, M.; Vairappan, C.S. Halogenated secondary metabolites from Japanese species of the red algal genus *Laurencia* (Rhodomelaceae, Ceramiales). *Curr. Top. Phytochem.* **2005**, *7*, 1–34.
80. Wang, B.-G.; Gloer, J.B.; Ji, N.-Y.; Zhao, J.-C. Halogenated Organic Molecules of Rhodomelaceae Origin: Chemistry and Biology. *Chem. Rev.* **2013**, *113*, 3632–3685. [\[CrossRef\]](#)
81. Suzuki, M.; Takahashi, Y.; Nakano, S.; Abe, T.; Masuda, M.; Ohnishi, T.; Noya, Y.; Seki, K.-I. An experimental approach to study the biosynthesis of brominated metabolites by the red algal genus *Laurencia*. *Phytochemistry* **2009**, *70*, 1410–1415. [\[CrossRef\]](#) [\[PubMed\]](#)
82. Young, D.N.; Howard, B.M.; Fenical, W. Subcellular localization of brominated secondary metabolites in the red alga *Laurencia snyderae*. *J. Phycol.* **1980**, *16*, 182–185. [\[CrossRef\]](#)
83. Vairappan, C.S.; Suzuki, M.; Abe, T.; Masuda, M. Halogenated metabolites with antibacterial activity from the Okinawan *Laurencia* species. *Phytochemistry* **2001**, *58*, 517–523. [\[CrossRef\]](#) [\[PubMed\]](#)
84. Cabrita, M.T.; Vale, C.; Rauter, A.P. Halogenated Compounds from Marine Algae. *Mar. Drugs* **2010**, *8*, 2301–2317. [\[CrossRef\]](#) [\[PubMed\]](#)
85. Juagdan, E.G.; Kalidindi, R.; Scheuer, P. Two new chamigranes from an hawaiian red alga *Laurencia cartilaginea*. *Tetrahedron* **1997**, *53*, 521–528. [\[CrossRef\]](#)
86. König, G.M.; Wright, A.D. *Laurencia rigida*: Chemical Investigations of Its Antifouling Dichloromethane Extract. *J. Nat. Prod.* **1997**, *60*, 967–970. [\[CrossRef\]](#)
87. Alarif, W.M.; Al-Lihaibi, S.S.; Abdel-Lateff, A.; Ayyad, S.-E.N. New Antifungal Cholestane and Aldehyde Derivatives from the Red Alga *Laurencia papillosa*. *Nat. Prod. Commun.* **2011**, *6*, 1821–1824. [\[CrossRef\]](#)
88. Li, Y.-X.; Li, Y.; Qian, Z.J.; Kim, M.M.; Kim, S.K. In Vitro Antioxidant Activity of 5-HMF Isolated from Marine Red Alga *Laurencia undulata* in Free-Radical-Mediated Oxidative Systems. *J. Microbiol. Biotechnol.* **2009**, *19*, 1319–1327. [\[CrossRef\]](#)

89. Topcu, G.; Aydogmus, Z.; Imre, S.; Gören, A.C.; Pezzuto, J.M.; Clement, J.A.; Kingston, D.G.I. Brominated Sesquiterpenes from the Red Alga *Laurencia obtusa*. *J. Nat. Prod.* **2003**, *66*, 1505–1508. [\[CrossRef\]](#)
90. Davyt, D.; Fernandez, R.; Suescun, L.; Mombrú, A.W.; Saldaña, J.; Domínguez, L.; Coll, J.; Fujii, M.T.; Manta, E. New Sesquiterpene Derivatives from the Red Alga *Laurencia scoparia*. Isolation, Structure Determination, and Anthelmintic Activity. *J. Nat. Prod.* **2001**, *64*, 1552–1555. [\[CrossRef\]](#)
91. Jung, W.-K.; Choi, I.; Oh, S.; Park, S.-G.; Seo, S.-K.; Lee, S.-W.; Lee, D.-S.; Heo, S.-J.; Jeon, Y.-J.; Je, J.-Y.; et al. Anti-asthmatic effect of marine red alga (*Laurencia undulata*) polyphenolic extracts in a murine model of asthma. *Food Chem. Toxicol.* **2009**, *47*, 293–297. [\[CrossRef\]](#) [\[PubMed\]](#)
92. Kurata, K.; Taniguchi, K.; Agatsuma, Y.; Suzuki, M. Diterpenoid feeding-deterrents from *Laurencia saitoi*. *Phytochemistry* **1998**, *47*, 363–369. [\[CrossRef\]](#)
93. Dembitsky, V.M.; Tolstikov, G.A. Natural halogenated sesquiterpens from marine organisms, chemistry for sustainable development. *Chem. Sustain. Dev.* **2004**, *12*, 1–12.
94. Suzuki, M.; Kurosawa, E.; Irie, T. Spirolaurenone, a new sesquiterpenoid containing bromine from *Laurencia glandulifera* Kützting. *Tetrahedron Lett.* **1970**, *11*, 4995–4998. [\[CrossRef\]](#)
95. Ji, N.-Y.; Li, X.-M.; Li, K.; Ding, L.-P.; Gloer, J.B.; Wang, B.-G. Diterpenes, Sesquiterpenes, and a C₁₅-Acetogenin from the Marine Red Alga *Laurencia mariannensis*. *J. Nat. Prod.* **2007**, *70*, 1901–1905. [\[CrossRef\]](#) [\[PubMed\]](#)
96. Li, X.-D.; Miao, F.-P.; Li, K.; Ji, N.-Y. Sesquiterpenes and acetogenins from the marine red alga *Laurencia okamurai*. *Fitoterapia* **2012**, *83*, 518–522. [\[CrossRef\]](#)
97. Liang, Y.; Li, X.-M.; Cui, C.-M.; Li, C.-S.; Sun, H.; Wang, B.-G. Sesquiterpene and Acetogenin Derivatives from the Marine Red Alga *Laurencia okamurai*. *Mar. Drugs* **2012**, *10*, 2817–2825. [\[CrossRef\]](#)
98. Liang, Y.; Li, X.M.; Cui, C.M.; Li, C.S.; Wang, B.G. A new rearranged chamigrane sesquiterpene from *Laurencia okamurai*. *Chin. Chem. Lett.* **2009**, *20*, 190–192. [\[CrossRef\]](#)
99. Li, X.-D.; Miao, F.-P.; Yin, X.-L.; Liu, J.-L.; Ji, N.-Y. Sesquiterpenes from the marine red alga *Laurencia composita*. *Fitoterapia* **2012**, *83*, 1191–1195. [\[CrossRef\]](#)
100. Ji, N.-Y.; Li, X.-M.; Wang, B.-G. Sesquiterpenes and Other Metabolites from the Marine Red Alga *Laurencia composita* (Rhodomelaceae). *Helv. Chim. Acta* **2010**, *93*, 2281–2286. [\[CrossRef\]](#)
101. Sims, J.J.; Lin, G.H.; Wing, R.M. Marine natural products X elatol, a halogenated sesquiterpene alcohol from the red alga *Laurencia elata*. *Tetrahedron Lett.* **1974**, *15*, 3487–3490. [\[CrossRef\]](#)
102. Lhullier, C.; Donnangelo, A.; Caro, M.; Palermo, J.A.; Horta, P.A.; Falkenberg, M.; Schenkel, E.P. Isolation of elatol from *Laurencia microcladia* and its palatability to the sea urchin *Echinometra lucunter*. *Biochem. Syst. Ecol.* **2009**, *37*, 254–259. [\[CrossRef\]](#)
103. González, A.; Darias, J.; Díaz, A.; Fourneron, J.; Martín, J.; Pérez, C. Evidence for the biogenesis of halogenated chamigrenes from the red alga *Laurencia obtusa*. *Tetrahedron Lett.* **1976**, *17*, 3051–3054. [\[CrossRef\]](#)
104. Vairappan, C.S. Potent antibacterial activity of halogenated metabolites from Malaysian red algae, *Laurencia majuscula* (Rhodomelaceae, Ceramiales). *Biomol. Eng.* **2003**, *20*, 255–259. [\[CrossRef\]](#)
105. Dos Santos, A.O.; Veiga-Santos, P.; Ueda-Nakamura, T.; Filho, B.P.D.; Sudatti, D.B.; Bianco, .M.; Pereira, R.C.; Nakamura, C.V. Effect of Elatol, Isolated from Red Seaweed *Laurencia dendroidea*, on *Leishmania amazonensis*. *Mar. Drugs* **2010**, *8*, 2733–2743. [\[CrossRef\]](#) [\[PubMed\]](#)
106. Desoti, V.C.; Lazarin-Bidóia, D.; Sudatti, D.B.; Pereira, R.C.; Alonso, A.; Ueda-Nakamura, T.; Dias Filho, B.P.; Nakamura, C.V.; De Oliveira Silva, S. Trypanocidal Action of (–)-Elatol Involves an Oxidative Stress Triggered by Mitochondria Dysfunction. *Mar. Drugs* **2012**, *10*, 1631–1646. [\[CrossRef\]](#)
107. Campos, A.; Souza, C.B.; Lhullier, C.; Falkenberg, M.; Schenkel, E.P.; Ribeiro-Do-Valle, R.M.; Siqueira, J.M. Anti-tumour effects of elatol, a marine derivative compound obtained from red algae *Laurencia microcladia*. *J. Pharm. Pharmacol.* **2012**, *64*, 1146–1154. [\[CrossRef\]](#) [\[PubMed\]](#)
108. Dias, D.A.; Urban, S. Phytochemical studies of the southern Australian marine alga, *Laurencia elata*. *Phytochemistry* **2011**, *72*, 2081–2089. [\[CrossRef\]](#) [\[PubMed\]](#)
109. Blunt, J.W.; Copp, B.R.; Munro, M.H.G.; Northcote, P.T.; Prinsep, M.R. Marine natural products. *Nat. Prod. Rep.* **2003**, *20*, 1–48. [\[CrossRef\]](#)
110. Dorta, E.; Díaz-Marrero, A.R.; Cueto, M.; D’croz, L.; Maté, J.L.; Darias, J. Chamigrenelactone, a polyoxygenated sesquiterpene with a novel structural type and devoid of halogen from *Laurencia obtusa*. *Tetrahedron Lett.* **2004**, *45*, 7065–7068. [\[CrossRef\]](#)
111. Brito, I.; Cueto, M.; Díaz-Marrero, A.R.; Darias, J.; San Martín, A. Oxachamigrenes, New Halogenated Sesquiterpenes from *Laurencia obtusa*. *J. Nat. Prod.* **2002**, *65*, 946–948. [\[CrossRef\]](#) [\[PubMed\]](#)
112. González, A.; Martín, J.; Martín, V.; Norte, M.; Pérez, R. Biomimetic approach to the synthesis of rhodolaureol and rhodolauradiol. *Tetrahedron Lett.* **1982**, *23*, 2395–2398. [\[CrossRef\]](#)
113. Suzuki, M.; Kurosawa, E.; Furusaki, A. The Structure and Absolute Stereochemistry of a Halogenated Chamigrene Derivative from the Red Alga *Laurencia* Species. *Bull. Chem. Soc. Jpn.* **1988**, *61*, 3371–3373. [\[CrossRef\]](#)
114. Ji, N.-Y.; Li, X.-M.; Li, K.; Wang, B.-G. Halogenated Sesquiterpenes from the Marine Red Alga *Laurencia saitoi* (Rhodomelaceae). *Helv. Chim. Acta* **2009**, *92*, 1873–1879. [\[CrossRef\]](#)
115. Howard, B.M.; Fenical, W. Structures and chemistry of two new halogen-containing chamigrene derivatives from *laurencia*. *Tetrahedron Lett.* **1971**, *16*, 1687–1690. [\[CrossRef\]](#)

116. Jongaramruong, J.; Blackman, A.J.; Skelton, B.W.; White, A.H. Chemical Relationships between the Sea Hare *Aplysia parvula* and the Red Seaweed *Laurencia filiformis* from Tasmania. *Aust. J. Chem.* **2002**, *55*, 275–280. [\[CrossRef\]](#)
117. Suzuki, M.; Daitoh, M.; Vairappan, C.S.; Abe, T.; Masuda, M. Novel Halogenated Metabolites from the Malaysian *Laurencia pannosa*. *J. Nat. Prod.* **2001**, *64*, 597–602. [\[CrossRef\]](#)
118. Suescun, L.; Mombrú, A.W.; Mariezcurrena, R.A.; Davyt, D.; Fernández, R.; Manta, E. Two natural products from the algae *Laurencia scoparia*. *Acta Crystallogr. Sect. C Cryst. Struct. Commun.* **2001**, *57*, 286–288. [\[CrossRef\]](#)
119. Francisco, M.E.Y.; Erickson, K.L. Ma'iliohydriin, a Cytotoxic Chamigrene Dibromohydriin from a Philippine *Laurencia* Species. *J. Nat. Prod.* **2001**, *64*, 790–791. [\[CrossRef\]](#)
120. Da Silva Machado, F.L.D.S.; Ventura, T.L.B.; Gestinari, L.M.d.S.; Cassano, V.; Resende, J.A.L.C.; Kaiser, C.R.; Lasunskia, E.B.; Muzitano, M.F.; Soares, A.R. Sesquiterpenes from the Brazilian Red Alga *Laurencia dendroidea*. *J. Agardh. Molecules* **2014**, *19*, 3181–3192. [\[CrossRef\]](#)
121. Rucker, R.; Kretzschmar, U. 9-Aristolene-1a-ol and 1,2,9,10-tetrahydroaristolane, new aristolane type sesquiterpenes. *Liebigs Ann. Chem.* **1971**, *748*, 214–217. [\[CrossRef\]](#)
122. Ji, N.-Y.; Li, X.-M.; Ding, L.-P.; Wang, B.-G. Aristolane Sesquiterpenes and Highly Brominated Indoles from the Marine Red Alga *Laurencia similis* (Rhodomelaceae). *Helv. Chim. Acta* **2007**, *90*, 385–391. [\[CrossRef\]](#)
123. Li, C.-S.; Li, X.-M.; Cui, C.-M.; Wang, B.-G. Brominated Metabolites from the Marine Red Alga *Laurencia similis*. *Z. Naturforsch.* **2010**, *65*, 87–89. [\[CrossRef\]](#)
124. Su, S.; Sun, W.-S.; Wang, B.; Cheng, W.; Liang, H.; Zhao, Y.-Y.; Zhang, Q.-Y.; Wu, J. A novel brominated cuparene-derived sesquiterpene ether from the red alga *Laurencia* sp. *J. Asian Nat. Prod. Res.* **2010**, *12*, 916–920. [\[CrossRef\]](#) [\[PubMed\]](#)
125. Kamada, T.; Vairappan, C.S. New Bioactive Secondary Metabolites from Bornean Red Alga, *Laurencia similis* (Ceramiales). *Nat. Prod. Commun.* **2013**, *8*, 287–288. [\[CrossRef\]](#)
126. Fraga, B.M. Natural sesquiterpenoids. *Nat. Prod. Rep.* **1997**, *14*, 145–162. [\[CrossRef\]](#)
127. Kladi, M.; Vagias, C.; Papazafiri, P.; Furnari, G.; Serio, D.; Roussis, V. New sesquiterpenes from the red alga *Laurencia microcladia*. *Tetrahedron* **2007**, *63*, 7606–7611. [\[CrossRef\]](#)
128. Yu, X.-Q.; He, W.-F.; Liu, D.-Q.; Feng, M.-T.; Fang, Y.; Wang, B.; Feng, L.-H.; Guo, Y.-W.; Mao, S.-C. A seco-laurane sesquiterpene and related laurane derivatives from the red alga *Laurencia okamurai* Yamada. *Phytochemistry* **2014**, *103*, 162–170. [\[CrossRef\]](#)
129. Davyt, D.; Fernandez, R.; Suescun, L.; Mombrú, A.W.; Saldaña, J.; Dominguez, L.; Fujii, M.T.; Manta, E. Bisabolanes from the red alga *Laurencia scoparia*. *J. Nat. Prod.* **2006**, *69*, 1113–1116. [\[CrossRef\]](#)
130. De Carvalho, L.T.; Fujii, M.T.; Roque, N.F.; Kato, M.J.; Lago, J.H.G. Aldingenin A, new brominated sesquiterpene from red algae *Laurencia aldingensis*. *Tetrahedron Lett.* **2003**, *44*, 2637–2640. [\[CrossRef\]](#)
131. de Carvalho, L.R.; Fujii, M.T.; Roque, N.F.; Lago, J.H.G. Aldingenin derivatives from the red alga *Laurencia aldingensis*. *Phytochemistry* **2006**, *67*, 1331–1335. [\[CrossRef\]](#)
132. Kladi, M.; Vagias, C.; Furnari, G.; Moreau, D.; Roussakis, C.; Roussis, V. Cytotoxic cuparene sesquiterpenes from *Laurencia microcladia*. *Tetrahedron Lett.* **2005**, *46*, 5723–5726. [\[CrossRef\]](#)
133. Mao, S.-C.; Guo, Y.-W. A Laurane Sesquiterpene and Rearranged Derivatives from the Chinese Red Alga *Laurencia okamurai* Yamada. *J. Nat. Prod.* **2006**, *69*, 1209–1211. [\[CrossRef\]](#)
134. Srikrishna, A.; Khan, I.; Babu, R.R.; Sajjanshetty, A. The first total synthesis of (±)-laurokamurene B. *Tetrahedron* **2007**, *63*, 12616–12620. [\[CrossRef\]](#)
135. Irie, T.; Suzuki, T.; Yasunari, Y.; Kurosawa, E.; Masamune, T. Laurene, a sesquiterpene hydrocarbon from *Laurencia* species. *Tetrahedron* **1969**, *25*, 459–468. [\[CrossRef\]](#) [\[PubMed\]](#)
136. Wratten, S.J.; Faulkner, D.J. Metabolites of the red alga *Laurencia subopposita*. *J. Org. Chem.* **1977**, *42*, 3343–3349. [\[CrossRef\]](#)
137. Alarif, W.M.; Al-Lihaibi, S.S.; Ayyad, S.-E.N.; Abdel-Rhman, M.H.; Badria, F.A. Laurene-type sesquiterpenes from the Red Sea red alga *Laurencia obtusa* as potential antitumor–antimicrobial agents. *Eur. J. Med. Chem.* **2012**, *55*, 462–466. [\[CrossRef\]](#)
138. Yamamura, S.; Hirata, Y. Structures of aplysin and aplysinol, naturally occurring bromo-compounds. *Tetrahedron* **1963**, *19*, 1485–1496. [\[CrossRef\]](#)
139. Elzen, G.W.; Williams, H.J.; Vinson, S.B. Isolation, identification and bioassay of cotton synomones mediating searching behavior by parasitoid *Campoletis sonorensis*. *J. Chem. Ecol.* **1984**, *10*, 1251–1264. [\[CrossRef\]](#) [\[PubMed\]](#)
140. Mao, S.-C.; Guo, Y.-W. Cuparene-Derived Sesquiterpenes from the Chinese Red Alga *Laurencia okamurai* Yamada. *Helv. Chim. Acta* **2005**, *88*, 1034–1039. [\[CrossRef\]](#)
141. Goldsmith, D.J.; John, T.K.; Kwong, C.D.; Painter, G.R. Preparation and rearrangement of trichothecane-like compounds. Synthesis of aplysin and filiformin. *J. Org. Chem.* **1980**, *45*, 3989–3993. [\[CrossRef\]](#)
142. Shizuri, Y.; Yamada, K. Laurebiphenyl, a dimeric sesquiterpene of the cyclolaurane-type from the red alga *Laurencia nidifica*. *Phytochemistry* **1985**, *24*, 1385–1386. [\[CrossRef\]](#)
143. Liang, Y.; Li, X.-M.; Li, C.-S.; Sun, H.; Wang, B.-G. Laurane-, Cyclolaurane-, and Cuparene-type Sesquiterpenes from the Marine Red Alga *Laurencia okamurai*. *Nat. Prod. Commun.* **2014**, *9*, 323–324. [\[CrossRef\]](#)
144. Sun, J.; Han, L.; Shi, D.; Ma, M.; Li, S.; Wang, S.; Han, L.; Yang, Y.; Fan, X.; Shi, J.; et al. Sesquiterpenes from Red Alga *Laurencia tristicha*. *J. Nat. Prod.* **2008**, *68*, 915–919, Erratum in *J. Nat. Prod.* **2008**, *71*, 296. [\[CrossRef\]](#) [\[PubMed\]](#)

145. Nemoto, H.; Nagamochi, M.; Ishibashi, H.; Fukumoto, K. A remarkable substituent effect on the enantioselectivity of tandem asymmetric epoxidation and enantiospecific ring expansion of cyclopropylidene alcohols: A new enantiocontrolled synthesis of (-)-debromoaplysin and (-)-aplysin. *J. Org. Chem.* **1994**, *59*, 74–79. [\[CrossRef\]](#)
146. Ji, N.-Y.; Li, X.-M.; Li, K.; Ding, L.-P.; Wang, B.-G. Laurane-derived sesquiterpenes from the marine red alga *Laurencia tristicha* (Rhodomelaceae). *Nat. Prod. Res.* **2008**, *22*, 715–718. [\[CrossRef\]](#)
147. Kazlauskas, R.; Murphy, P.; Quinn, R.; Wells, R. New laurene derivatives from *Laurencia filiformis*. *Aust. J. Chem.* **1976**, *29*, 2533–2539. [\[CrossRef\]](#)
148. Dias, D.A.; White, J.M.; Urban, S. *Laurencia Filiformis*: Phytochemical Profiling by Conventional and HPLC-NMR Approaches. *Nat. Prod. Commun.* **2009**, *4*, 157–172. [\[CrossRef\]](#)
149. Appleton, D.R.; Babcock, R.C.; Copp, B.R. Novel tryptophan-derived dipeptides and bioactive metabolites from the sea hare *Aplysia dactylomela*. *Tetrahedron* **2001**, *57*, 10181–10189. [\[CrossRef\]](#)
150. König, G.M.; Wright, A.D. New C₁₅ Acetogenins and Sesquiterpenes from the Red Alga *Laurencia* sp. cf. *L. gracilis*. *J. Nat. Prod.* **1994**, *57*, 477–485. [\[CrossRef\]](#)
151. Kladi, M.; Xenaki, H.; Vagias, C.; Papazafiri, P.; Roussis, V. New cytotoxic sesquiterpenes from the red algae *Laurencia obtusa* and *Laurencia microcladia*. *Tetrahedron* **2006**, *62*, 182–189. [\[CrossRef\]](#)
152. Iliopoulou, D.; Roussis, V.; Pannecouque, C.; De Clercq, E.; Vagias, C. Halogenated sesquiterpenes from the red alga *Laurencia obtusa*. *Tetrahedron* **2002**, *58*, 6749–6755. [\[CrossRef\]](#)
153. Aydoğmuş, Z.; Imre, S.; Ersoy, L.; Wray, V. Halogenated secondary metabolites from *Laurencia Obtusa*. *Nat. Prod. Res.* **2004**, *18*, 43–49. [\[CrossRef\]](#) [\[PubMed\]](#)
154. Brennan, M.R.; Erickson, K.L. Austradiol acetate and austradiol diacetate, 4,6-dihydroxy-(+)-selinane derivatives from an Australian *Laurencia* sp. *J. Org. Chem.* **1982**, *47*, 3917–3921. [\[CrossRef\]](#)
155. Kazlauskas, R.; Murphy, P.; Wells, R.; Daly, J.; Oberhansli, W. Heterocladol, a halogenated selinane sesquiterpene of biosynthetic significance from the red alga *Laurencia filiformis*: Its isolation, crystal structure and absolute configuration. *Aust. J. Chem.* **1977**, *30*, 2679–2687. [\[CrossRef\]](#)
156. Guella, G.; Skropeta, D.; Mancini, I.; Pietra, F. The First 6,8-Cycloeudesmane Sesquiterpene from a Marine Organism: The Red Seaweed *Laurencia microcladia* from the Baia di Calenzana, Elba Island. *Z. Für Naturforschung B* **2002**, *57*, 1147–1151. [\[CrossRef\]](#)
157. Suzuki, M.; Takahashi, Y.; Mitome, Y.; Itoh, T.; Abe, T.; Masuda, M. Brominated metabolites from an Okinawan *Laurencia intricata*. *Phytochemistry* **2002**, *60*, 861–867. [\[CrossRef\]](#)
158. Reward, B.M.; Fenical, W. α - and β -snyderol; new bromo-monocyclic sesquiterpenes from the seaweed *Laurencia*. *Tetrahedron Lett.* **1976**, *17*, 41–44. [\[CrossRef\]](#)
159. Su, H.; Shi, D.-Y.; Li, J.; Guo, S.-J.; Li, L.-L.; Yuan, Z.-H.; Zhu, X.-B. Sesquiterpenes from *Laurencia similis*. *Molecules* **2009**, *14*, 1889–1897. [\[CrossRef\]](#)
160. Kuniyoshi, M.; Marma, M.S.; Higa, T.; Bernardinelli, G.; Jefford, C.W. New Bromoterpenes from the Red Alga *Laurencia luzonensis*. *J. Nat. Prod.* **2001**, *64*, 696–700. [\[CrossRef\]](#)
161. Kuniyoshi, M.; Wahome, P.G.; Miono, T.; Hashimoto, T.; Yokoyama, M.; Shrestha, K.L.; Higa, T. Terpenoids from *Laurencia luzonensis*. *J. Nat. Prod.* **2005**, *68*, 1314–1317. [\[CrossRef\]](#) [\[PubMed\]](#)
162. Su, H.; Yuan, Z.-H.; Li, J.; Guo, S.-J.; Deng, L.-P.; Han, L.-J.; Zhu, X.-B.; Shi, D.-Y. Sesquiterpenes from the Marine Red Alga *Laurencia saitoi*. *Helv. Chim. Acta* **2009**, *92*, 1291–1297. [\[CrossRef\]](#)
163. Makhani, D.S.; Yokoyama, M.; Miono, T.; Maesato, T.; Maedomari, M.; Wisespongpan, P.; Kuniyoshi, M. New sesquiterpenes from the Okinawan red alga *Laurencia luzonensis*. *Bull. Fac. Sci. Univ. Ryukyus* **2006**, *81*, 115–120.
164. Vairappan, C.S.; Kamada, T.; Lee, W.-W.; Jeon, Y.-J. Anti-inflammatory activity of halogenated secondary metabolites of *Laurencia snackeyi* (Weber-van Bosse) Masuda in LPS-stimulated RAW 264.7 macrophages. *J. Appl. Phycol.* **2013**, *25*, 1805–1813. [\[CrossRef\]](#)
165. Wijesinghe, W.; Kim, E.-A.; Kang, M.-C.; Lee, W.-W.; Lee, H.-S.; Vairappan, C.S.; Jeon, Y.-J. Assessment of anti-inflammatory effect of 5 β -hydroxypalisadin B isolated from red seaweed *Laurencia snackeyi* in zebrafish embryo in vivo model. *Environ. Toxicol. Pharmacol.* **2014**, *37*, 110–117. [\[CrossRef\]](#) [\[PubMed\]](#)
166. Su, H.; Yuan, Z.; Li, J.; Guo, S.; Han, L.; Zhu, X.; Shi, D. [Studies on chemical constituents of *Laurencia saitoi*]. *Zhongguo Zhong Yao Za Zhi* **2009**, *34*, 871–874.
167. Wright, A.D.; Goclik, E.; König, G.M. Three New Sesquiterpenes from the Red Alga *Laurencia perforata*. *J. Nat. Prod.* **2003**, *66*, 435–437. [\[CrossRef\]](#)
168. Vairappan, C.S.; Suzuki, M.; Ishii, T.; Okino, T.; Abe, T.; Masuda, M. Antibacterial activity of halogenated sesquiterpenes from Malaysian *Laurencia* spp. *Phytochemistry* **2008**, *69*, 2490–2494. [\[CrossRef\]](#)
169. Erickson, K.L.; Beutler, J.A.; Gray, G.N.; Cardellina, J.H.; Boyd, M.R. Majapolene A, a Cytotoxic Peroxide, and Related Sesquiterpenes from the Red Alga *Laurencia majuscula*. *J. Nat. Prod.* **1995**, *58*, 1848–1860. [\[CrossRef\]](#)
170. Monde, K.; Taniguchi, T.; Miura, N.; Vairappan, C.S.; Suzuki, M. Absolute configurations of brominated sesquiterpenes determined by vibrational circular dichroism. *Chirality* **2006**, *18*, 335–339. [\[CrossRef\]](#)
171. Da Silva, F.L.M.; Pacienza-Lima, W.; Rossi-Bergmann, B.; de Souza, L.M.G.; Fujii, M.T.; Campos de Paula, J.; Costa, S.S.; Lopes, N.P.; Kaiser, C.R.; Soares, A.R. Antileishmanial Sesquiterpenes from the Brazilian Red Alga *Laurencia dendroidea*. *Planta Med.* **2010**, *77*, 733–735. [\[CrossRef\]](#)

172. Al-Massarani, S. Phytochemical and Biological Properties of Sesquiterpene Constituents From the Marine Red Seaweed *Laurencia*: A Review. *Nat. Prod. Chem. Res.* **2014**, *2*, 147. [CrossRef]
173. Wang, B.; Svetlov, V.; Wolf, Y.I.; Koonin, E.V.; Nudler, E.; Artsimovitch, I. Allosteric Activation of SARS-CoV-2 RNA-Dependent RNA Polymerase by Remdesivir Triphosphate and Other Phosphorylated Nucleotides. *mBio* **2021**, *12*, e0142321. [CrossRef] [PubMed]
174. National Center for Biotechnology Information Protein Database. Available online: <http://www.ncbi.nlm.nih.gov/protein/> (accessed on 10 March 2023).
175. Yin, W.; Mao, C.; Luan, X.; Shen, D.-D.; Shen, Q.; Su, H.; Wang, X.; Zhou, F.; Zhao, W.; Gao, M.; et al. Structural basis for inhibition of the RNA-dependent RNA polymerase from SARS-CoV-2 by remdesivir. *Science* **2020**, *368*, 1499–1504. [CrossRef]
176. Kim, S.; Thiessen, P.A.; Bolton, E.E.; Chen, J.; Fu, G.; Gindulyte, A.; Han, L.; He, J.; He, S.; Shoemaker, B.A.; et al. PubChem substance and compound databases. *Nucleic Acids Res.* **2016**, *44*, D1202–D1213. [CrossRef]
177. Pence, H.E.; Williams, A. ChemSpider: An Online Chemical Information Resource. *J. Chem. Educ.* **2010**, *87*, 1123–1124. [CrossRef]
178. Lyu, C.; Chen, T.; Qiang, B.; Liu, N.; Wang, H.; Zhang, L.; Liu, Z. CMNPD: A comprehensive marine natural products database towards facilitating drug discovery from the ocean. *Nucleic Acids Res.* **2020**, *49*, D509–D515. [CrossRef] [PubMed]
179. Biovia, D.S. Discovery Studio. Available online: <https://discover.3ds.com/discovery-studio-visualizer-download> (accessed on 15 December 2022).
180. Avogadro: An Open-Source Molecular Builder and Visualization Tool. Version 1.95. Available online: <http://avogadro.cc/> (accessed on 23 November 2022).
181. Hanwell, M.D.; Curtis, D.E.; Lonie, D.C.; Vandermeersch, T.; Zurek, E.; Hutchison, G.R. Avogadro: An advanced semantic chemical editor, visualization, and analysis platform. *J. Cheminform.* **2012**, *4*, 17. [CrossRef] [PubMed]
182. Guex, N.; Peitsch, M.C. SWISS-MODEL and the Swiss-Pdb Viewer: An environment for comparative protein modeling. *Electrophoresis* **1997**, *18*, 2714–2723. [CrossRef]
183. Morris, G.M.; Huey, R.; Lindstrom, W.; Sanner, M.F.; Belew, R.K.; Goodsell, D.S.; Olson, A.J. AutoDock4 and AutoDockTools4: Automated docking with selective receptor flexibility. *J. Comput. Chem.* **2009**, *30*, 2785–2791. [CrossRef]
184. Eberhardt, J.; Santos-Martins, D.; Tillack, A.F.; Forli, S. AutoDock Vina 1.2.0: New Docking Methods, Expanded Force Field, and Python Bindings. *J. Chem. Inf. Model.* **2021**, *61*, 3891–3898. [CrossRef]
185. Trott, O.; Olson, A.J. AutoDock Vina: Improving the speed and accuracy of docking with a new scoring function, efficient optimization, and multithreading. *J. Comput. Chem.* **2010**, *31*, 455–461. [CrossRef]
186. Kuriata, A.; Gierut, A.M.; Oleniecki, T.; Ciemny, M.P.; Kolinski, A.; Kurcinski, M.; Kmiecik, S. CABS-flex 2.0: A web server for fast simulations of flexibility of protein structures. *Nucleic Acids Res.* **2018**, *46*, W338–W343. [CrossRef] [PubMed]
187. Banerjee, P.; Eckert, A.O.; Schrey, A.K.; Preissner, R. ProTox-II: A webserver for the prediction of toxicity of chemicals. *Nucleic Acids Res.* **2018**, *46*, W257–W263. [CrossRef] [PubMed]
188. Borba, J.V.; Alves, V.M.; Braga, R.C.; Korn, D.R.; Overdahl, K.; Silva, A.C.; Hall, S.U.; Overdahl, E.; Braga, R.; Kleinstreuer, N.; et al. STopTox: An in Silico Alternative to Animal Testing for Acute Systemic and Topical Toxicity. *Environ. Health Perspect.* **2022**, *130*, 27012. [CrossRef] [PubMed]
189. Daina, A.; Michielin, O.; Zoete, V. SwissADME: A free web tool to evaluate pharmacokinetics, drug-likeness and medicinal chemistry friendliness of small molecules. *Sci. Rep.* **2017**, *7*, 42717. [CrossRef] [PubMed]
190. Zhao, Y.H.; Abraham, M.H.; Le, J.; Hersey, A.; Luscombe, C.N.; Beck, G.; Sherborne, B.; Cooper, I. Rate-Limited Steps of Human Oral Absorption and QSAR Studies. *Pharm. Res.* **2002**, *19*, 1446–1457. [CrossRef]
191. Husain, A.; Ahmad, A.; Alam Khan, S.; Asif, M.; Bhutani, R.; Al-Abbasi, F.A. Synthesis, molecular properties, toxicity and biological evaluation of some new substituted imidazolidine derivatives in search of potent anti-inflammatory agents. *Saudi Pharm. J.* **2016**, *24*, 104–114. [CrossRef]
192. Filimonov, D.A.; Lagunin, A.A.; Glorizova, T.A.; Rudik, A.V.; Druzhilovskii, D.S.; Pogodin, P.V.; Poroikov, V.V. Prediction of the Biological Activity Spectra of Organic Compounds Using the Pass Online Web Resource. *Chem. Heterocycl. Compd.* **2014**, *50*, 444–457. [CrossRef]
193. Gao, Y.; Yan, L.; Huang, Y.; Liu, F.; Zhao, Y.; Cao, L.; Wang, T.; Sun, Q.; Ming, Z.; Zhang, L.; et al. Structure of the RNA-dependent RNA polymerase from COVID-19 virus. *Science* **2020**, *368*, 779–782. [CrossRef]
194. Begum, F.; Srivastava, A.K.; Ray, U. Repurposing nonnucleoside antivirals against SARS-CoV2 NSP12 (RNA dependent RNA polymerase): In silico-molecular insight. *Biochem. Biophys. Res. Commun.* **2021**, *571*, 26–31. [CrossRef] [PubMed]
195. Mosayebnia, M.; Bozorgi, A.H.; Rezaeiannpour, M.; Kobarfard, F. In silico prediction of SARS-CoV-2 main protease and polymerase inhibitors: 3D-Pharmacophore modelling. *J. Biomol. Struct. Dyn.* **2022**, *40*, 6569–6586. [CrossRef] [PubMed]
196. Tungary, E.; Wahjudi, M.; Kok, T. Secondary Metabolites of Various Indonesian Medicinal Plants as SARS-CoV-2 Inhibitors: In Silico Study. *MPI Media Pharm. Indones.* **2022**, *4*, 136–146. [CrossRef]
197. Ikeguchi, M.; Ueno, J.; Sato, M.; Kidera, A. Protein Structural Change Upon Ligand Binding: Linear Response Theory. *Phys. Rev. Lett.* **2005**, *94*, 078102. [CrossRef]
198. Agoni, C. The Binding of Remdesivir to SARS-CoV-2 RNA-Dependent RNA Polymerase May Pave The Way Towards the Design of Potential Drugs for COVID-19 Treatment. *Curr. Pharm. Biotechnol.* **2021**, *22*, 1520–1537. [CrossRef]
199. Mishra, A.; Rathore, A.S. RNA dependent RNA polymerase (RdRp) as a drug target for SARS-CoV2. *J. Biomol. Struct. Dyn.* **2022**, *40*, 6039–6051. [CrossRef]

200. Arora, S.; Lohiya, G.; Moharir, K.; Shah, S.; Yende, S. Identification of Potential Flavonoid Inhibitors of the SARS-CoV-2 Main Protease 6YNQ: A Molecular Docking Study. *Digit. Chin. Med.* **2020**, *3*, 239–248. [[CrossRef](#)]
201. Umar, A.K. Flavonoid compounds of buah merah (*Pandanus conoideus* Lamk) as a potent SARS-CoV-2 main protease inhibitor: In silico approach. *Futur. J. Pharm. Sci.* **2021**, *7*, 158–159. [[CrossRef](#)]
202. Ortega, J.T.; Jastrzebska, B.; Rangel, H.R. Omicron SARS-CoV-2 Variant Spike Protein Shows an Increased Affinity to the Human ACE2 Receptor: An In Silico Analysis. *Pathogens* **2021**, *11*, 45. [[CrossRef](#)]
203. Katuwal, S.; Upadhyaya, S.R.; Marahatha, R.; Shrestha, A.; Regmi, B.P.; Khadayat, K.; Basnet, S.; Basnyat, R.C.; Parajuli, N. In Silico Study of Coumarins: Wedelolactone as a Potential Inhibitor of the Spike Protein of the SARS-CoV-2 Variants. *J. Trop. Med.* **2023**, *2023*, 4771745. [[CrossRef](#)]
204. Pokharkar, O.; Lakshmanan, H.; Zyryanov, G.; Tsurkan, M. In Silico Evaluation of Antifungal Compounds from Marine Sponges against COVID-19-Associated Mucormycosis. *Mar. Drugs* **2022**, *20*, 215. [[CrossRef](#)] [[PubMed](#)]
205. Tang, Y.; Liu, J.; Zhang, D.; Xu, Z.; Ji, J.; Wen, C. Cytokine Storm in COVID-19: The Current Evidence and Treatment Strategies. *Front. Immunol.* **2020**, *11*, 1708. [[CrossRef](#)] [[PubMed](#)]
206. Cron, R.Q.; Caricchio, R.; Chatham, W.W. Calming the cytokine storm in COVID-19. *Nat. Med.* **2021**, *27*, 1674–1675. [[CrossRef](#)] [[PubMed](#)]

Disclaimer/Publisher’s Note: The statements, opinions and data contained in all publications are solely those of the individual author(s) and contributor(s) and not of MDPI and/or the editor(s). MDPI and/or the editor(s) disclaim responsibility for any injury to people or property resulting from any ideas, methods, instructions or products referred to in the content.